Title page

GPR30 in spinal cholecystokinin-positive neurons modulates neuropathic pain

Qing Chen[1#], Hui Wu[1#], Shulan Xie[1,2#], Fangfang Zhu[1], Fang Xu[3], Qi Xu[1], Lihong Sun[1], Yue Yang[4], Linghua Xie[1], Jiaqian Xie[5], Hua Li[1], Ange Dai[1], Wenxin Zhang[1], Luyang Wang[1], Cuicui Jiao[1], Honghai Zhang[4], Xuelong Zhou[1], Zhen-Zhong Xu[2,6,7**], Xinzhong Chen[1*].

[1]Department of Anesthesia, Women's Hospital, Zhejiang University School of Medicine, Hangzhou, 310006, China.

[2]NANHU Brain-Computer Interface Institute, Hangzhou, 311100, China.

[3]Department of Anesthesiology, The Second Affiliated Hospital, Chongqing Medical University, Chongqing, 400010, China.

[4]Department of Anesthesiology, Affiliated Hangzhou First People's Hospital, Westlake University School of Medicine, Hangzhou, 310006, China.

[5]Department of Anesthesiology, Sir Run Run Shaw Hospital, School of Medicine, Zhejiang University, Hangzhou, 317500, China.

[6]Department of Anesthesiology, First Affiliated Hospital and School of Brain Science and Brain Medicine, Zhejiang University School of Medicine, Hangzhou, 310058, China.

[7]Liangzhu Laboratory, MOE Frontier Science Center for Brain Science and Brain-machine Integration, State Key Laboratory of Brain-machine Intelligence, NHC and CAMS Key Laboratory of Medical Neurobiology, Zhejiang University, Hangzhou, 311121, China

[#]These authors contributed equally.

***Correspondence:** Chen Xinzhong, M.D., Department of Anesthesia, Women's Hospital, Zhejiang University School of Medicine, Hangzhou, 310006, China.

E-mail: chenxinz@zju.edu.cn. Tel: +86-571-87061501.

Fax: +86-571-87061878

****Correspondence:** Xu Zhen-Zhong, PhD, Department of Neurobiology and Anesthesiology of First Affiliated Hospital, Zhejiang University School of Medicine, Hangzhou, 310058, China

E-mail: xuzz@zju.edu.cn

Abstract

Neuropathic pain, a major health problem affecting 7-10% of the global population, lacks effective treatment due to its elusive mechanisms. Cholecystokinin-positive (CCK^+) neurons in the spinal dorsal horn (SDH) are critical for neuropathic pain, yet the underlying molecular mechanisms remain unclear. Here, we show that the membrane estrogen receptor G-protein coupled estrogen receptor (GPER/GPR30) in spinal neurons was significantly upregulated in chronic constriction injury (CCI) mice and that inhibition of GPR30 in CCK^+ neurons reversed CCI-induced neuropathic pain. Furthermore, GPR30 in spinal CCK^+ neurons was essential for the enhancement of AMPA-mediated excitatory synaptic transmission in CCI mice. Moreover, GPR30 was expressed in spinal CCK^+ neurons that received direct projection from the primary sensory cortex (S1-SDH). Chemogenetic inhibition of S1-SDH post-synaptic neurons alleviated CCI-induced neuropathic pain. Conversely, chemogenetic activation of these neurons mimicked neuropathic pain symptoms, which were attenuated by spinal inhibition of GPR30. Finally, we confirmed that GPR30 in S1-SDH post-synaptic neurons was required for CCI-induced neuropathic pain. Taken together, our findings suggest that GPR30 in spinal CCK^+ neurons is pivotal for neuropathic pain and GPR30 mediates descending facilitation by corticospinal direct projections, thereby representing a promising therapeutic target for neuropathic pain.

Key words: GPR30; neuropathic pain; spinal CCK positive neurons; corticospinal direct projections; descending facilitation

Introduction

Neuropathic pain, a persistent and disabling condition affecting approximately 7–10% of the global population, arises from a lesion or dysfunction of the somatosensory nervous system [1-4]. This disorder manifests as mechanical allodynia (pain triggered by innocuous stimuli) and thermal hyperalgesia (exaggerated pain responses to noxious heat)[1, 5, 6]. However, the complex and elusive mechanisms of neuropathic pain still make it difficult to treat. Therefore, identifying precise mechanisms and discovering new therapeutic targets is urgently needed.

The spinal cord (SC) serves as a pivotal hub for processing peripheral sensory inputs and integrating descending modulatory signals. Neuropathic mechanical allodynia occurs via circuit-based transformation in this region[4, 5, 7, 8]. Superficial laminae of the SC primarily encode noxious stimuli, whereas deeper laminae process innocuous signals. Under neuropathic conditions, however, low-threshold mechanosensory inputs aberrantly activate nociceptive neurons in superficial laminae through disinhibition and sensitization mechanisms, driving mechanical allodynia. Excitatory interneurons, constituting ~75% of spinal dorsal horn (SDH) neurons, are central to this pathological process[9-11]. Among these, cholecystokinin-expressing (CCK^+) interneurons, enriched in SDH deep laminae, have recently been proposed as mediators of both mechanical and thermal hypersensitivity[10, 12]. Notably, CCK^+ neurons receive direct corticospinal projections from the primary sensory cortex (S1), modulating neuropathic pain sensitivity[13]; however, the molecular underpinnings of this regulation remain obscure.

Estrogen, beyond its classical nuclear receptors (ERα/ERβ), exerts non-genomic effects via the membrane receptor G protein-coupled estrogen receptor (GPR30), which is increasingly recognized as a key player in nociceptive modulation[14-26]. Although GPR30's role in pain

modulation has been documented, its specific contribution to SDH circuitry in neuropathic pain remains unexplored.

In this study, we demonstrate that spinal GPR30 orchestrates neuropathic pain by modulating excitability of CCK^+ neurons and corticospinal descending facilitation. We discovered that GPR30 activation in spinal CCK^+ neurons was both required and sufficient for the development of neuropathic pain. Interestingly, we observed that GPR30 in spinal CCK^+ neurons was required for the enhancement of spontaneous excitatory post-synaptic currents (sEPSC) in CCI mice, in an AMPA-dependent manner. Importantly, we revealed that GPR30 was expressed in the spinal CCK^+ neurons receiving direct projections from S1 sensory cortex, and that GPR30 in S1-SDH post-synaptic neurons was critical for CCI-induced neuropathic pain. These findings establish GPR30 in spinal CCK^+ neurons as a compelling therapeutic target for neuropathic pain management.

Results

Spinal inhibition of GPR30 reverses CCI-induced neuropathic pain and neuronal activation

To investigate the functional relevance of spinal GPR30 in neuropathic pain, we employed a chronic constriction injury (CCI) model to evaluate whether pharmacological blockade of spinal GPR30 alleviates neuropathic pain (Fig 1A). Quantitative PCR (qPCR) analysis revealed a significant elevation of *Gper1* (GPR30) mRNA levels in the lumbar spinal dorsal horn (SDH) of CCI mice compared to sham (Fig 1B). By the way, the *Gper1* mRNA levels in the DRG remained unchanged after CCI (Fig 1B). Intrathecal application of the GPR30 antagonist, G-15, effectively attenuated CCI-induced mechanical allodynia and thermal hyperalgesia in both sexes of mice (Fig 1C-E), whereas basal nociceptive thresholds remained unaltered in naïve mice (Fig S1A and B). Of note, the analgesic effects of G-15 lasted for up to 6 hours after intrathecal application in CCI mice (Fig S1C). Immunochemical data demonstrated that innocuous tactile stimulation triggered pronounced c-Fos expression, a marker of neuronal activation, predominantly in GPR30^{+} cells within the SDH of CCI mice (Fig 1F-J). Critically, G-15 treatment substantially suppressed this c-Fos expression (Fig 1F-J), indicating that spinal GPR30 inhibition normalizes both hypersensitivity and neuronal activation in neuropathic pain in both sexes.

We further probed whether GPR30 activation alone could mimic neuropathic symptoms in naïve mice. Intrathecal application of the selective GPR30 agonist, G-1, robustly evoked mechanical allodynia and thermal hypersensitivity, with symptom persistence exceeding 48 hours (Fig S1D-G). Consistent with behavioral outcomes, G-1 administration markedly increased c-Fos^{+} neuron density in the SDH, with over 80% of activated cells co-expressing

GPR30.

Collectively, these findings establish spinal GPR30 as a critical mediator of sex-independent neuropathic pain development in the CCI model.

GPR30 in spinal CCK$^+$ neurons is required for CCI-induced neuropathic pain

To delineate the spinal cellular substrates of GPR30-mediated pain modulation, we first mapped its expression pattern. Our results revealed exclusive GPR30 localization to neuronal populations within the SDH instead of astrocytes or microglial cells via immunochemistry (Fig. S2). Notably, as an estrogen receptor, GPR30 expression showed no sexual dimorphism (Fig S2D). To assess the relative expression of GPR30 in excitatory versus inhibitory neurons, we performed *Ish* and immunostaining with *VGAT*, *Vglut2* and GPR30 (Fig 2A). GPR30 was predominantly expressed on the excitatory neurons of SDH (Fig 2B). Further characterization in wild-type mice using AAV2/9-Camk2-mCherry labeling also confirmed predominant GPR30 enrichment in SDH excitatory interneurons (Fig S3).

Given the established role of CCK$^+$ neurons in neuropathic pain and their dominance among SDH excitatory interneurons[10, 21, 27, 28], we hypothesized that GPR30 within this subset drives nociceptive sensitization. To validate this, we characterized CCK expression in the spinal cord via transgenic models by crossing *CCK-Cre* with *Ai14* reporter mice (Fig 2C). *Ish* and immunostaining confirmed that our transgenic mice recapitulated the majority of *CCK* expression in the deep laminae of the SDH as marked by isolectin B4 (IB4), CGRP and NF200 (Fig 2D and E). To verify the role of CCK$^+$ neurons in allodynia under neuropathic pain, we performed immunostaining of c-Fos in CCK-Ai14 mice, and we confirmed that more CCK$^+$ neurons were activated after CCI (Fig S4). What's more, near-universal CCK$^+$ neurons were

co-localized with GPR30 (Fig 2F and G).

To functionally interrogate GPR30 and CCK^+ neurons in neuropathic pain, we injected AAV2/9-DIO-shGper1-EGFP into lumbar SDH of *CCK-Cre* mice for conditional knock-down of *Gper1*, and 3 weeks later we subjected mice to CCI as well as subsequent behavioral tests (Fig 3A). Viral targeting accuracy was verified by immunostaining showing deep laminae-specific expression, mirroring endogenous CCK^+ neurons distribution (Fig 3B). CCI-induced *Gper1* mRNA upregulation was significantly blunted in knockdown mice (Fig 3C, Fig S5A), confirming the transcriptional efficacy of virus.

Behavioral tests revealed that *Gper1* knockdown in CCK^+ neurons attenuated CCI-induced mechanical allodynia and thermal hyperalgesia across sexes, without altering basal nociceptive thresholds (Fig 3D-F). To dissect affective components of neuropathic pain, we used real-time PEA test with innocuous mechanical stimulation as shown before[2] (Fig 3G). Scramble-treated CCI mice exhibited persistent aversion to stimulated side, whereas *Gper1* knockdown abolished this aversive behavior during post-stimulation period (Fig 3H-L).

GPR30 in spinal CCK^+ neurons is essential for the enhancement of excitatory synaptic transmission in the SDH of CCI mice

To investigate the role of GPR30 expressed on CCK^+ neurons in neuropathic pain transmission, we conducted electrophysiological recordings using whole-cell patch clamp recording on fluorescently labeled neurons in spinal slices from CCI or sham-operated *CCK-Cre* mice treated with shRNA (Fig 4A and B). Since a significant proportion of spinal CCK^+ neurons form excitatory synapses with upstream neurons, we focused on recording postsynaptic currents from GFP-labeled CCK^+ neurons in laminae III-V approximately two weeks after CCI surgery. As

154 hypothesized, the amplitude of excitatory postsynaptic currents (EPSCs) in CCK^+ neurons was
155 significantly enhanced in CCI mice compared to sham mice, although the frequency remained
156 unchanged (Fig 4C-E). Notably, this enhancement in amplitude was abolished in *Gper1*
157 knockdown mice (Fig 4C, E). It is worth mentioning that inhibitory postsynaptic currents
158 (IPSCs) also contribute to the regulation of neuronal excitability. However, our findings
159 indicated that knockdown of *Gper1* did not affect the IPSCs of spinal CCK^+ neurons in CCI
160 mice (Fig S5B-D).

161 Given that EPSCs are primarily mediated through glutamatergic receptors such as AMPA
162 receptor, coupled with emerging evidence showing that GPR30 could facilitate excitatory
163 transmission via increasing the clustering of glutamatergic receptor subunits[25], we proceeded
164 to examine whether GPR30-mediated EPSCs depend on AMPA-mediated currents.
165 Electrophysiological experiments were carried out in spinal slices from *CCK-Cre* mice treated
166 with intraspinal injections of AAV2/9-DIO-EGFP (Fig 4F). To record AMPA-dependent
167 currents, electronical stimulation from the electrode placed in the deep laminae of SDH was
168 applied (Fig 4G). And CCK^+ neurons were held at -70 mV in the presence of APV (100 μM) to
169 block NMDA receptors and bicuculline (20 μM) to block $GABA_A$ receptors and strychnine (0.5
170 μM) to block glycine receptors. All recorded cells responded to the electrode stimulation,
171 exhibiting evoked EPSCs (Fig 4H and I). Furthermore, the application of 0.1 μM G-1
172 augmented the amplitude of AMPA currents (Fig 4H and I). These findings collectively suggest
173 that GPR30 regulates EPSCs in CCK^+ neurons through an AMPA-dependent mechanism.

174 **GPR30 is expressed in the spinal CCK^+ neurons receiving direct projection from S1 cortex**

175 To anatomically verify that the lumbar spinal cord receives direct descending projections from

the S1 cortex, we employed a combination of retrograde and anterograde tracing methods to investigate the connections between cortical neurons and their axonal innervation in the SDH. Our results revealed that retrograde labeling with cholera toxin subunit B-555 (CTB-555), injected into the deep laminae of the lumbar SDH, predominantly localized neurons in the contralateral S1 cortex (Fig 5A-C). Of note, the neurons projecting from S1 cortex are primarily excitatory pyramidal neurons located in layer V[29]. Similarly, fiber tracing using AAV2/9-hSyn-EGFP indicated that axons from S1 terminate extensively in laminae III-V of the contralateral SDH (Fig 5D-F).

Building on previous findings suggesting a functional interaction between S1-SDH projections and spinal CCK^+ neurons[13], our current study aimed to further elucidate the structural relationship among GPR30, S1-SDH projections and CCK^+ neurons. To achieve this, we performed anterograde trans-monosynaptic tracing by injecting AAV2/1-hSyn-Cre into the right S1 cortex, followed by AAV2/9-DIO-mCherry into the contralateral lumbar SDH. This approach allowed us to visualize the $mCherry^+$ S1-SDH postsynaptic neurons in the deep laminae of the lumbar SDH (Fig 5G and H). Consistent with prior observations, we found that these SDH downstream neurons exhibited colocalization with CCK^+ neurons, with 28.1% of $mCherry^+$ neurons expressing CCK (Fig 5I and J). Thus, our findings confirm that spinal CCK^+ neurons are directly innervated by the S1 cortex.

To further examine the interplay between GPR30, S1-SDH projections, and CCK^+ neurons, we utilized a monosynaptic anterograde tracing strategy. Specifically, we injected AAV2/1-EF1α-FLP into the right S1 cortex and AAV2/9-hSyn-Con/Fon-GFP into the contralateral lumbar SDH of CCK-Cre mice. This strategy enabled us to visualize GFP-positive S1-SDH

postsynaptic CCK^+ neurons (Fig. 5K and L). Our co-staining results revealed that the vast majority of CCK^+ S1-SDH postsynaptic neurons expressed GPR30 (Fig 5M and N). These data collectively indicate that the majority of CCK^+ neurons receiving S1 projections express GPR30.

GPR30 in S1-SDH post-synaptic neurons is critical for CCI-induced neuropathic pain

Given that GPR30 has been verified to be expressed on CCK^+ neurons receiving S1-SDH direct projections (Fig 5M), we employed a combination of chemogenetic and pharmacological approaches to determine whether neurons innervated by S1-SDH direct projections mediate nociception via GPR30[30]. Specifically, we performed injections of anterograde AAV2/1-hSyn-Cre into the right S1 WT mice. One week later, we administered AAV2/9-hSyn-DIO-hM3Dq (Gq)-mCherry into the lumbar SDH (Fig 6A). Pharmacological activation of these post-synaptic neurons with CNO in Gq-treated mice significantly induced spontaneous pain-like behaviors, such as paw scratching, biting, and licking, in the hind paws and tails (Fig 6B). Furthermore, chemogenetic activation of S1-SDH post-synaptic neurons dramatically induced mechanical allodynia and thermal hyperalgesia in both sexes compared to negative control groups (Fig 6C-E). Notably, the reduction in nociceptive thresholds could be effectively reversed by intrathecal administration of G-15 (Fig 6C-E). The corresponding immunohistochemistry results using c-Fos confirmed the chemogenetic activation of S1-SDH post-synaptic neurons, which could be suppressed by intrathecal application of G-15 (Fig 6F-H).

To further explore the role of S1-SDH post-synaptic neurons in the modulation of neuropathic pain, we employed chemogenetic inhibitory methods to suppress these neurons in

220 CCI mice (Fig S6A). The suppression of S1-SDH post-synaptic neurons could dramatically
221 relieve the mechanical allodynia and thermal hyperalgesia induced by CCI (Fig S6B-D). To
222 establish the essential role of GPR30 in this process, we specifically knocked down the
223 expression of *Gper1* on S1-SDH post-synaptic neurons and subjected mice to CCI after
224 adequate viral expression (Fig 7A). Interestingly, the knockdown of *Gper1* in S1-SDH post-
225 synaptic neurons was sufficient to relieve mechanical allodynia and thermal hyperalgesia in
226 both sexes (Fig 7B-D). Immunochemistry showed the viral location in deep laminae of SDH
227 (Fig 7E) and qPCR confirmed the suppression of *Gper1* mRNA expression which was increased
228 by CCI (Fig 7F). Collectively, these findings underscore the critical role of GPR30 in the
229 descending facilitation of S1-SDH direct projections in the neuropathic pain.

230 **Discussion**

231 CCK^+ neurons, located in the deep laminae of the spinal cord, have long been recognized for
232 their pivotal role in the development and maintenance of neuropathic pain, as well as
233 descending facilitation by sensory cortex-spinal cord projections. Despite extensive research,
234 the molecular mechanisms underlying nociception remain poorly understood. GPR30, as a
235 membrane estrogen receptor, exerts modulatory effects on various physiological and
236 pathological processes, including the development of neuropathic pain, within seconds to
237 minutes [22]. In this study, we observed significant upregulation of GPR30 expression in the
238 SDH after CCI, underscoring its critical role in neuropathic pain development. To investigate
239 this further, we employed a comprehensive approach, including transgenic mice models,
240 behavioral assays, pharmacological interventions, chemogenetic methods, and
241 electrophysiological studies. These experiments revealed that GPR30 plays an indispensable

role in neuropathic pain, particularly through its regulation of AMPA-dependent EPSCs in spinal CCK^+ neurons, which are essential for pain signaling. Furthermore, we demonstrated that GPR30 is crucial for the descending facilitation of pain signals via corticospinal direct projections. These findings collectively suggest that GPR30 in spinal CCK^+ neurons may represent a promising therapeutic target for neuropathic pain.

Estrogen has long been recognized as a key player in modulating nociception, with its drastic fluctuations notably impacting nociceptive thresholds[31]. Our prior research demonstrated that moderate estrogen supplementation effectively mitigated hyperalgesia in ovariectomized (OVX) mice, however, excessive estrogen supplementation paradoxically exacerbated hyperalgesia[31]. This discrepancy might stem from the fact that varying estrogen concentrations can differentially activate estrogen receptors, including nuclear receptors (ERα and ERβ) and membrane receptors (GPR30)[22]. Considering our findings that inhibiting spinal GPR30 does not alter the basal nociception in naïve mice, it appears that GPR30 may not be significantly activated by estrogen under normal conditions. Additionally, estrogen has long been implicated in modulating neuropathic pain. Intra-dorsal root ganglion (DRG) administration of estrogen in CCI rats has been shown to enhance mechanical and thermal pain in an ERα-dependent manner[32]. Conversely, estrogen supplementation in the anterior cingulate cortex (ACC) of CCI mice significantly alleviated neuropathic hyperalgesia in a GPR30-dependent manner[33]. These findings further underscore the distinct roles of different estrogen receptors in pain modulation.

GPR30 is widely expressed in the nervous system and exerts vital effects in nociceptive modulation[16, 23, 24, 33-37]. For example, the activation of GPR30 in DRG could aggravate the

hyperalgesia in OVX mice, while inhibition of GPR30 relieved hyperalgesia[38]. Besides, the GPR30 expressed on GABAergic cells in rostral ventromedial medulla (RVM) mediates the descending facilitation of nociception[24]. However, though GPR30 is also widely expressed in SDH[26], still little is known about the functions as well as underlying mechanisms of spinal GPR30 in nociceptive modulation. Consistent with previous studies[39], here we found that intrathecal injection of G-1 could dramatically induce mechanical allodynia and thermal hyperalgesia in mice. To further explore whether spinal GPR30 is involved in pathological nociception, we subjected mice to CCI surgery to mimic neuropathic pain[2, 40]. In accordance with our expectations, the inhibition of spinal GPR30 significantly reversed the mechanical allodynia and thermal hyperalgesia induced by CCI. Moreover, GPR30 has been reported to be involved in nociceptive sexual dimorphism. For example, the regulatory role of GPR30 in DRG in maintenance of hyperalgesia induced by repeated exposure of opioid only exists in female rats[41, 42]. However, according to our results, spinal GPR30 modulated nociception in a sex-independent manner. We also found that GPR30 is indiscriminately expressed on the neurons of both sexes of mice, which might account for the sex-independent function of spinal GPR30 in nociceptive modulation. Consistent with our results, several studies also have confirmed that the spinal *Gper1* expression showed no significant difference between male and female mice[43]. What's more, the fluctuation of estrogen failed to change the basic expression of spinal GPR30[31]. These results further indicate that spinal GPR30 modulated nociception in a sex-independent manner.

The SDH is a major locus for the integration of peripheral sensory input and supraspinal modulation. Most peripheral nociceptive afferents project to the superficial laminae of the SDH

286 which respond to the noxious stimulations, while low-threshold mechanoreceptors form
287 synaptic contacts in the deep laminae which respond to innocuous stimulations[8]. However,
288 under the condition of mechanical allodynia, innocuous stimulation might also activate more
289 superficial nociceptive circuits and lead to painful perception, which might come from the
290 circuit-based transformation in the SDH[6, 44]. It should be noted that the spinal dorsal horn is
291 composed of a large number of excitatory (75%) and inhibitory (25%) interneurons, as well as
292 a small part of projection neurons which relay integrated information to various supraspinal
293 regions[9]. Excitatory interneurons have been confirmed to take a vital role in conveying
294 mechanical allodynia according to the nature of injury[10, 45]. As a distinct type of excitatory
295 interneurons mainly located in the deeper laminae of SDH, CCK^+ neurons are important for
296 neuropathic injuries[10-12]. The inhibition of spinal CCK^+ neurons could alleviate neuropathic
297 mechanical allodynia to a great extent[10]. By the way, spinal CCK^+ neurons also account for
298 the thermal hyperalgesia[12]. However, little is known how CCK^+ neurons mediate the
299 nociception. Combined with our results that GPR30 is widely expressed in spinal excitatory
300 interneurons and involved in neuropathic pain modulation, we speculate that CCK^+ neurons
301 might convey neuropathic hyperalgesia via GPR30. As expected, most CCK^+ neurons express
302 GPR30 and knock-down of the *Gper1* in CCK^+ neurons dramatically relieve the pain induced
303 by CCI, thus indicating the vital role of GPR30 in CCK^+ neurons mediating neuropathic pain.
304 However, it should be noted that half of $GPR30^+$ neurons are not co-localized with CCK^+
305 neurons, and further studies are needed to explore the function of these $GPR30^+CCK^-$ neurons
306 in neuropathic pain.

307 Abnormal activation of neurons in SDH is one of the causes of hyperalgesia and the change

308 of post synaptic currents is the vital factor influencing neuronal excitability[46, 47]. Given this
309 critical link between EPSCs and excitability, we measured excitatory postsynaptic currents
310 (EPSCs) and found an elevation of EPSCs amplitudes in spinal CCk^+ neurons after CCI,
311 indicating the increased excitability of CCK^+ neurons in CCI mice. Furthermore, the knock-
312 down of *Gper1* in CCK^+ neurons could inhibit the increase of EPSCs amplitude induced by
313 CCI. Together, these data illustrate that GPR30 take a vital role in activation of CCK^+ neurons
314 after nerve injury via promoting the enhancement of EPSCs. It should be noted that EPSCs are
315 specifically produced by glutamatergic receptors expressed on post-synaptic membrane,
316 including AMPA and NMDA receptors[25, 46, 48]. In our study, we confirmed that the selective
317 activation of GPR30 by G-1 remarkedly enhanced the AMPA-current in spinal CCK^+ neurons,
318 which might account for the increased excitability of CCK^+ neurons in neuropathic pain. It
319 should be noted that the IPSCs could also influence the excitability of neurons, however, the
320 knockdown of Gper1 failed to change the IPSCs amplitude in CCI mice, suggesting that GPR30
321 did not take part in the inhibitory synaptic regulation.

322 Increasing evidence has mapped neural circuits from peripheral to central nervous system
323 to illustrate the neural mechanisms of nociception[5, 7-9, 45, 49]. In brief, pain is derived from the
324 activation of peripheral nociceptors whose cell bodies lie in DRG, and then nociceptive signals
325 are transduced to the SDH for preliminary regulation and finally projected to cerebral cortex
326 via a series of brain region mediating nociception. Additionally, pain is also modulated by the
327 descending modulatory pathways constituted of projections from ventrolateral periaqueductal
328 gray (PAG) to the RVM and then to the spinal cord which takes several steps[50-55]. However, A
329 recent study has come up with the existence of long direct projections form S1 cortex to deep

laminae of SDH and the vital role of S1-SDH projections in neuropathic pain[13]. Inhibition of S1-SDH projections attenuates neuropathic pain, while activation decreases pain thresholds in naive mice. We confirmed the existence of these direct projections and their postsynaptic targets' critical role in neuropathic pain. Notably, these long projections specifically synapse within SDH deep laminae onto CCK^+ neurons[13].We also structurally verify that CCK^+ neurons receive direct projections from S1 cortex. Furthermore, we also found that the majority of CCK^+ neurons receiving S1-SDH projections express GPR30, thus indicating an important role of GPR30 in descending modulation of S1-SDH. As expected, the knockdown of *Gper1* in S1-SDH post-synaptic neurons dramatically alleviated the hyperalgesia induced by CCI. All these results further confirmed an important role of GPR30 in descending facilitation of neuropathic pain. However, since viral strategy only labeled a small fraction of post-synaptic CCK^+ neurons from S1 cortex and was insufficient to functionally manipulate these neurons, more efficient methods should be employed to verify the role of GPR30 expressed on S1-SDH post-synaptic CCK^+ neurons under neuropathic pain conditions.

Conclusion

GPR30 plays a critical role in the development of neuropathic pain, particularly within CCK+ neurons. Our research highlights GPR30's essential function in enhancing AMPA-dependent EPSCs, which are crucial for the activation of CCK^+ neurons and the subsequent development of abnormal nociception under neuropathic conditions. Furthermore, GPR30 is pivotal in facilitating the descending projections via corticospinal projections, contributing to the propagation of neuropathic pain signals. These findings suggest that targeting GPR30 in spinal CCK^+ neurons could be a promising therapeutic strategy for neuropathic pain in clinic.

352 **Materials and methods**

353 **Animals**

354 Mice of both sexes ranging in age from 8 weeks to 12 weeks were used for this study, including
355 C57BL/6JRJ wild-type (purchased from SLAC Laboratory Animal CO. LTD, Shanghai, China),
356 *CCK-Cre* mice and *Ai14* mice (originally purchased from Jackson Laboratory). In accordance
357 with the Jackson Laboratory's protocol, transgenic mice were genotyped. All animals were kept
358 in a humidity-controlled room with free access to food and water, the facility was maintained
359 at 22 ℃ and ran on 12 hours of light/dark cycles. A random assignment of animals to different
360 experiment groups was conducted. The animals were treated in accordance with protocols
361 approved by the Animal Ethic and Welfare Committee of Zhejiang University School of
362 Medicine, and all experimental procedures were carried out in accordance with the National
363 Institute of Health Guide for Care and Use of Laboratory Animals (NIH Publications NO.86-
364 23).

365 **Drug administration**

366 For pharmacological manipulation of the activity of spinal GPR30, G-1 or G-15 (diluent of 0.2
367 mg/mL, administration of 100 μg/kg, 10 μL per mice; APExBIO, USA) was dissolved in 1%
368 DMSO with Saline and administered intrathecally as previously described[39]. To be specific,
369 mice were lightly anesthetized with 1.5% inhaled isoflurane, and held with a pen under the
370 pelvis while a 25-gauge needle attached to a 10-μL syringe (Hamilton, Nevada, USA) was
371 inserted in the subarachnoid space between vertebrae L5 and L6 until a tail flick was observed.
372 The syringe was held for 30 seconds after the injection of 10 μL solution per mice. For
373 chemogenetic manipulation of S1-SDH post-synaptic neurons, Clozapine N-oxide (CNO; 2.5

374 mg/kg, 150 μL per mice; MCE, China) was dissolved in saline with gentle vortex for mixing
375 and then administered intraperitoneally [30]. The behavioral assessments were carried out 30
376 minutes following the injection.

377 **Virus and CTB microinjection**

378 For intracranial injection, mice were anesthetized with 1% pentobarbital sodium solution (70
379 mg/kg per mice) and then secured in a stereotaxic frame (RWD Life Science, Shenzhen, China).
380 A middle scalp incision exposed the skull, and then a hole was drilled on the skull above the
381 right S1 cortex to allow passage of a glass microelectrode filled with the virus. Viral injections
382 were performed with the following coordinates of S1: 0.95~1.15 mm from bregma, 1.4~1.6
383 mm from midline, and 0.9~1.1 mm ventral to skull. A volume of 300 nL virus was injected at
384 50 nL/min with calibrated glass microelectrodes by a microsyringe pump (#78-8710 KD
385 Scientific, USA). After infusion, the micropipette was slowly removed after five minutes. For
386 spinal cord injection, mice were anesthetized with 1% pentobarbital sodium solution. The spinal
387 cord could be visible between T12 and T13 vertebral spines following a middle incision along
388 the lumbar vertebrae. With a stereotaxic frame, a glass microelectrode was inserted between
389 L3-L4 spinal cord to a depth of -400 um below the dura, avoiding the posterior spinal arteries.
390 With a stereotaxic injector, 500 nL of viral solution or CTB-555 (1% in PBS; BrainVTA, Wuhan,
391 China) was slowly infused over a period of 5 minutes. The micropipette was left in place for 5
392 minutes after infusion before being slowly removed.

393 For knock-down the *Gper1* in CCK^+ neurons, AAV2/9-CMV-DIO-(EGFP-U6)-shRNA
394 (GPR30)-WPRE-pA (5×10^{12} v.g./mL) or AAV2/9-CMV-DIO-(EGFP-U6)-shRNA (Scramble)-
395 WPRE-pA (5×10^{12} v.g./mL) was injected into the lumbar SDH of *CCK-Cre* mice. For

visualization of the CCK+ neurons, AAV2/9-CMV-DIO-EGFP-WPRE-pA (5.2×10^{12} v.g./mL) was injected into the lumbar SDH of *CCK-Cre* mice. For anterograde tracing of S1 cortex projections, AAV2/9-hSyn-EGFP-WPRE (1×10^{13} v.g./mL) was in injected into the S1 cortex of wild type mice. For visualization of the S1-SDH post-synaptic neurons, AAV2/1-hSyn-CRE-WPRE-pA (1×10^{13} v.g./mL) was injected into the S1 cortex and AAV2/9-EF1α-DIO-mCherry-WPRE-pA (1×10^{13} v.g./mL) was injected into the lumbar SDH in wild type mice. For visualization of CCK^{+} post-synaptic neurons of S1-SDH projections, AAV2/1- EF1α-FLP-WPRE-pA (1×10^{13} v.g./mL) was injected into the S1 cortex and AAV2/8-hSyn-Con/Fon-EYFP-WPRE-pA (2×10^{12} v.g./mL) was injected into the lumbar SDH of *CCK-Cre* mice. For chemogenetic manipulation of S1-SDH post-synaptic neurons, AAV2/1-hSyn-CRE-WPRE-pA (1×10^{13} v.g./mL) was injected into the S1 cortex, while AAV2/9-hSyn-DIO-hM3Dq (Gq)-mCherry (3.3×10^{13} v.g./mL; dilution: 1:5) or AAV2/9-hSyn-DIO-hM4Di (Gi)-mCherry (3.3×10^{13} v.g./mL; dilution: 1:5) or AAV2/9-hSyn-DIO-mCherry (3×10^{13} v.g./mL; dilution: 1:5) was injected into the lumbar SDH in wild type mice. All viruss mentioned above were purchased from BrainVTA (Wuhan, China). For visualization of the localization of excitatory interneurons in the SDH, AAV2/9-hSyn-mCaMkIIa-mCherry-WPRE-pA (1×10^{13} v.g./mL; Taitool Bioscience, Shanghai, China) was injected into the lumbar SDH of wild type mice.

For structural tests, at least 3 mice were examined and each mouse was examined at least 3 slices. For behavioral tests, at least 6 mice per group were examined. The mice with improper position or expression of virus were excluded.

Chronic constriction injury (CCI)

The CCI-induced neuropathic pain model was employed as previously documented [2], Mice

418 were lightly anesthetized via inhaled 1.5% Isoflurane. An incision was made on the skin of each
419 mouse, exposing the sciatic nerve. Four ligations with 6-0 chromic silk were loosely tied around
420 the sciatic nerve. Nerve constriction should be minimal until a brief twitch can be observed. In
421 sham mice, the sciatic nerve was exposed without ligation. The animal was allowed to recover
422 from surgery for 2 weeks before behavioral testing.

423 **Behavioral test**

424 ***Punctate mechanical stimuli (von Frey filaments):*** Mice were habituated to opaque cage
425 (7.5×15×15 cm) for 1 hour the day before and 30min immediately prior to testing. Testing was
426 performed using a series of von Frey filaments using the Dixon's Up-down method[56],
427 beginning with the 0.16 g filament. The 50% paw withdrawal threshold was determined for
428 each mouse on one hind paws. Each filament was gently applied to the plantar surface of the
429 hind paw for 5 seconds or until a response such as a sharp withdraw, shaking or licking of the
430 limb was observed. Between individual measurement, filaments were applied at least 3 minutes
431 after the mice had returned to their initial resting state.

432 ***Dynamic mechanical stimuli (Brush):*** Each mouse was habituated in an opaque cage
433 (7.5×15×15 cm) for 1 hour the day before and 30 minutes immediately prior to testing. The
434 plantar hind paw was stimulated by light stroking from heel to toe with a paintbrush. A positive
435 response was recorded if the animal lifting, shaking or licking the limb. The application was
436 repeated 10 times with a 3 minutes interval between each stimulation.

437 ***Plantar heat test (Hargreaves Method):*** Mice were placed in an acrylic chamber on a glass
438 table and allowed to acclimate to the test chamber for 1hour the day before and 30 minutes
439 immediately prior to testing. The thermal paw withdrawal latency was assessed using the

plantar test (Ugo Basile Biological Research Apparatus, Gemonio, Italy). While the mouse was in a motionless state, a radiant heat source, which was maintained at 40 W, was applied to the plantar surface of the mouse's paw through the glass plate. The paw withdrawal latency was defined as the time to withdrawal of the hind paw from the heat source, and 15 seconds was used as the cut-off to avoid injury.

Real-time place escape/avoidance test (RT-PEA)

Each mouse was habituated in the test room for 1 hour the day before and 30 minutes immediately prior to testing. The Real-time place escape/avoidance chamber (50×28×32 cm; made with plastic plates that had distinct color with another) was placed on the mesh floor. The tested mouse was placed in a two-chamber box and allowed to explore both chambers without any stimulation (pre-stimulation, 10 minutes); mechanical simulation by 0.16 g von Frey filament was intermittently delivered whenever the mouse entered or stayed in the preferred chamber, as shown in the pre-stimulation stage (stimulation, 10 minutes); the mouse then freely explored the box without any stimulation (post-stimulation, 10 minutes). The mouse's movements and time stay in preferred chamber were recorded via an ANY-Maze system.

Immunohistochemistry

Mice were deeply anesthetized with 1% pentobarbital sodium solution and then perfused with phosphate-buffered saline (PBS) followed by pre-cooled 4% paraformaldehyde fix solution (PFA). For c-Fos staining, Von Frey filament with the same force (0.16 g) representing light mechanical stimulation was applied to the right hind paw of each group every 30 s for 20 min. Then animals were then perfused with PBS and 4% PFA ninety minutes after Von Frey filament stimulation. Tissue were harvested and post-fixed in PFA at 4°C over night before being

462 dehydrated in 30% sucrose for 2days. Tissues were embedded in Optimal Cutting temperature
463 (OCT) and then cut into 10-30 μm sections placed directly onto slides. Tissue slices were
464 blocked at room temperature for an hour with block solution containing 10% normal donkey
465 serum (NDS), 1% bovine serum albumin BSA and 0.3% triton X-100 in PBS (PBS-T), and then
466 incubated with primary antibodies diluted in 1% NDS, 1% BSA in PBS-T at 4℃ overnight.
467 Sections were washed in PBS and incubated with secondary antibodies at room temperature for
468 1-2 hours. Slices were washed and covered with Fluoromount-G containing DAPI. All images
469 were taken with an Olympus FV1000 confocal microscope. Antibodies used were as follows:
470 anti-c-Fos (1:1000, guinea pig, Oasis Biofarm, Hangzhou, China), anti-GPR30 (1:500, rabbit,
471 Alomone Labs, Isreal) , anti-IBA1 (1:1000, goat, Novusbio, USA), anti-GFAP (1:1000, mouse,
472 Cell Signaling Technology, USA), IB4-FITC (1:1000, Thermofisher, USA), Nissl (1:500,
473 Thermofisher, USA), goat anti-guinea pig IgG-488 (1:500, Oasis Biofarm, Hangzhou, China),
474 donkey anti-rabbit IgG-488 (1:500, Thermofisher, USA), donkey anti-rabbit IgG-555 (1:500,
475 Thermofisher, USA), donkey anti-mouse IgG-488 (1:500, Thermofisher, USA), donkey anti-
476 goat IgG-488 (1:500, Abcam, USA).

477 ***In Situ* Hybridization**

478 To verify the specificity of transgenic mice, *In situ* hybridization was performed according to
479 the manufacturer's instructions from RNAscope® Multiplex Fluorescent Reagent Kit v2
480 (Advanced Cell diagnostics, USA) with custom-designed probe for *CCK* (Mm-CCK-C1,
481 Advanced Cell diagnostics, USA). According to the protocols, coronal lumbar spinal sections
482 (10 μm) collected and used for fluorescence in situ hybridization to detect CCK^{+} neurons. The
483 slice used to stain RFP primary antibody and *CCK* probe were taken from the -80 °C refrigerator

484 and immediately incubated with pre-cooled 4% PFA for 15 minutes, followed by gradient
485 dehydration (50% ethanol, 70% ethanol, 100% ethanol and 100% ethanol, 5 min for each
486 gradient). The slides were then incubated with RNAscope® hydrogen peroxide at room
487 temperature for 10 minutes, rinsed with distilled water and PBS. Anti-RFP primary antibody
488 (1:1000, rabbit, Rockland, USA) prepared with co-detection diluent (323180, Advanced Cell
489 Diagnostics) was then added to the slices and incubated overnight at 4 °C for subsequent in situ
490 hybridization staining. To characterized the specific expression of GPR30 in SDH, VGAT (Mm-
491 VGAT-C1) and Vglut2 (Mm-Slc17a6-C2) probe were used as described above as well as anti-
492 GPR30 primary antibody (1:250). At least 3 mice were examined and each mouse was
493 examined at least 3 slices in these experiments.

494 **Real-time PCR**

495 Mice lumbar spinal cords or DRG were collected on day 4 after CFA and on day 14 after CCI.
496 Tissues were rapidly collected, frozen in liquid nitrogen and stored at -80°C. RNA was extracted
497 with standard procedures using FastPure Cell/Tissue Total RNA Isolation Kit V2 (Vazyme,
498 Nanjing, China). 500ng of total RNA from each sample was reverse-transcribed with HiScript
499 III RT SuperMix for qPCR (+gDNA wiper) (Vazyme, Nanjing, China). Expression of each
500 mRNA was quantified using ChamQ Universal SYBR qPCR Master Mix (Vazyme, Nanjing,
501 China). The sequences of quantitative PCR primers were as follows: *Gper1*: F:
502 CCTCTGCTACTCCCTCATCG, R: ACTATGTGGCCTGTCAAGGG; GAPDH: F:
503 AAGAAGGTGGTGAAGCAGGCATC, R: CGGCATCGAAGGTGGAAGATG.

504 **Spinal slice preparation and whole-cell recording**

505 Spinal slices were prepared as previously described[57]. Mice (6-8-week-old, 2 weeks after CCI

surgery) were anesthetized with 1% pentobarbital sodium solution and perfused with ice-cold oxygenated (95% O_2 and 5% CO_2) cutting artificial cerebrospinal fluid (ACSF, in mM: 100 sucrose, 63 NaCl, 2.5 KCl, 1.2 NaH_2PO_4, 1.2 $MgCl_2$, 25 glucose, and 25 $NaHCO_3$), and the spinal cord was rapidly removed. Transverse spinal cord slices (300 μm, L4 to L6 segment) were prepared using a vibratome (VT1200S, Leica, Germany) and incubated in oxygenated NMDG-ACSF (in mM: 93 NMDG, 2.5 KCl, 1.2 NaH_2PO4, 30 $NaHCO_3$, 20 HEPES, 25 Glucose, 5 Na ascorbate, 2 thiourea, 3 Na pyruvate, 10 $MgSO_4$ and 0.5 $CaCl_2$, and adjusted to pH 7.4 with HCl) at 34 °C for 15 min. The slices were then transferred to normal ACSF (in mM: 125 NaCl, 2.5 KCl, 1.25 NaH_2PO_4, 1.2 $MgCl_2$, 2.5 $CaCl_2$, 25 glucose, and 11 $NaHCO_3$) at 34 °C for 1h and maintained at room temperature before recording. The slices were transferred to a recording chamber perfused with normal ACSF saturated with 95% O_2 and 5% CO_2.

Whole-cell patch- clamp recordings were performed using a Heka EPC 10 amplifier (Heka Elektronik). Borosilicate glass pipettes with the resistance of 3-5 MΩ were pulled using a horizontal pipette puller (P97, Sutter instruments, USA). The pipettes were filled with cesium-based intracellular fluid (in mM: 100 $CsCH_3SO_3$, 20 KCl, 10 HEPES, 4 Mg-ATP, 0.3 Tris-GTP, 7 $Tris_2$-Phosphocreatine, 3 QX-314; pH 7.3, 285–290 mOsm). Targeted whole-cell recordings were made from EGFP expressing neurons in slices taken from *CCK-Cre* mice with virus injection. For spontaneous excitatory post synaptic currents (sEPSCs) recording, the membrane potential was held at -70 mV, and for spontaneous inhibitory post synaptic currents (sIPSCs) recording, the membrane potential was held at +10 mV. Then sEPSCs and sIPSCs were recorded for 100s and analyzed using MiniAnalysis software (Synaptosoft). 5 mice per group

528 were examined in the experiment.

529 To record AMPA-mediated EPSCs, an electrode placed in the deep laminae of SDH were
530 stimulated at every 15 seconds, and the CCK^+ neurons were voltage clamped at -70 mV.
531 Meanwhile, the spinal slices were incubated with ACSF containing APV (100 μM) to block
532 NMDA receptors and bicuculline (20 μM) and strychnine (0.5 μM) to block inhibitory synaptic
533 events. AMPAR-mediated EPSCs were recorded for 15 consecutive responses after stable
534 baseline before and after G-1 application (0.1 μM) to compare to effect of G-1 on AMPAR-
535 mediated EPSCs. 4 mice examined in the experiment.

536 **Statistical analyses**

537 All experiments were randomized. Animals were randomly chosen from multiple cages. For
538 behavior experiments, measurements were taken blinded to condition. All data are reported as
539 mean ± SEM. The required sample sizes were estimated on the basis of our past experience.
540 Statistical analysis was performed using GraphPad Prism V6. Normal distribution was
541 performed using SPSS V20. For all experiments, $P<0.05$ was considered to be statistically
542 significant.

543 **Acknowledgements**

544 This work was supported by the National Natural Science Foundation of China grants
545 (82371220) and 4+X Clinical Research Project of Women's Hospital, School of Medicine,
546 Zhejiang University (ZDFY2022-4XA102). This work was also supported by the Fundamental
547 Research Funds for the Central Universities (2023ZFJH01-01, 2024ZFJH01-01, and 226-2022-
548 00227). We also thank Sanhua Fang from the Core Facilities, Zhejiang University School of
549 Medicine for their excellent technical assistant.

Conflict of Interest

The authors declare that they have no competing interests.

Author contributions

X.Z.C. and Z.Z.X. conceived the study. Q.C., H.W., S.L.X., J.Q.X., L.H.X., H.L., F.F.Z., conducted the experiments and collected data. Q.C., H.W., and S.L.X. analyzed the data. Y.Y. and H.H.Z. draw the graphic abstract and revise the manuscript. A.G.D., F.X., W.X.Z., L.H.S., Q.X., L.Y.W. and C.C.J. assisted with animal maintenance and provided reagents. Q.C., X.L.Z., Z.Z.X. and X.Z.C. drafted the article. All authors approved the version to be submitted.

Data availability

The data that support the findings of this study are available on request from the corresponding author.

Reference

[1] GHAZISAEIDI S, MULEY M M, SALTER M W. Neuropathic Pain: Mechanisms, Sex Differences, and Potential Therapies for a Global Problem [J]. Annu Rev Pharmacol Toxicol, 2023, 63: 565-83.

[2] XIA L P, LUO H, MA Q, et al. GPR151 in nociceptors modulates neuropathic pain via regulating P2X3 function and microglial activation [J]. Brain, 2021, 144(11): 3405-20.

[3] COHEN S P, VASE L, HOOTEN W M. Chronic pain: an update on burden, best practices, and new advances [J]. Lancet, 2021, 397(10289): 2082-97.

[4] BANNISTER K, SACHAU J, BARON R, et al. Neuropathic Pain: Mechanism-Based Therapeutics [J]. Annu Rev Pharmacol Toxicol, 2020, 60: 257-74.

[5] FINNERUP N B, KUNER R, JENSEN T S. Neuropathic Pain: From Mechanisms to Treatment [J]. Physiol Rev, 2021, 101(1): 259-301.

[6] LOLIGNIER S, EIJKELKAMP N, WOOD J N. Mechanical allodynia [J]. Pflugers Arch, 2015, 467(1): 133-9.

[7] CHENG L, DUAN B, HUANG T, et al. Identification of spinal circuits involved in touch-evoked dynamic mechanical pain [J]. Nat Neurosci, 2017, 20(6): 804-14.

[8] OSSIPOV M H, LAI J, MALAN T P, JR., et al. Spinal and supraspinal mechanisms of neuropathic pain [J]. Ann N Y Acad Sci, 2000, 909: 12-24.

[9] SEAL C P A R P. Neural circuits for pain: Recent advances and current views [J]. Science, 2016, 354(6312): 578-84.

[10] PEIRS C, WILLIAMS S G, ZHAO X, et al. Mechanical Allodynia Circuitry in the Dorsal Horn Is Defined by the Nature of the Injury [J]. Neuron, 2021, 109(1): 73-90 e7.

[11] ABRAIRA V E, KUEHN E D, CHIRILA A M, et al. The Cellular and Synaptic Architecture of the Mechanosensory Dorsal Horn [J]. Cell, 2017, 168(1-2): 295-310 e19.

[12] WANG H, CHEN W, DONG Z, et al. A novel spinal neuron connection for heat sensation [J]. Neuron, 2022, 110(14): 2315-33 e6.

[13] LIU Y, LATREMOLIERE A, LI X, et al. Touch and tactile neuropathic pain sensitivity are set by corticospinal projections [J]. Nature, 2018, 561(7724): 547-50.

[14] LI L H, LING D D, LIN H, et al. Ovariectomy induces hyperalgesia accompanied by upregulated estrogen receptor alpha and protein kinase B in the rat spinal cord [J]. Physiol Behav, 2023, 271: 114342.

[15] LEE J, CHUNG S, HWANG M, et al. Estrogen Mediates the Sexual Dimorphism of GT1b-Induced Central Pain Sensitization [J]. Cells, 2023, 12(5).

[16] XU Z, XIE W, FENG Y, et al. Positive interaction between GPER and beta-alanine in the dorsal root ganglion uncovers potential mechanisms: mediating continuous neuronal sensitization and neuroinflammation responses in neuropathic pain [J]. J Neuroinflammation, 2022, 19(1): 164.

[17] VANNUCCINI S, CLEMENZA S, ROSSI M, et al. Hormonal treatments for endometriosis: The endocrine background [J]. Rev Endocr Metab Disord, 2022, 23(3): 333-55.

[18] SHARP J L, PEARSON T, SMITH M A. Sex differences in opioid receptor mediated effects: Role of androgens [J]. Neurosci Biobehav Rev, 2022, 134: 104522.

[19] TRAMULLAS M, COLLINS J M, FITZGERALD P, et al. Estrous cycle and ovariectomy-induced changes in visceral pain are microbiota-dependent [J]. iScience, 2021, 24(8): 102850.

[20] PANG H, CHEN S, KLYNE D M, et al. Low back pain and osteoarthritis pain: a perspective of

estrogen [J]. Bone Res, 2023, 11(1): 42.
[21] DUAN L L, QIU X Y, WEI S Q, et al. Spinal CCK contributes to somatic hyperalgesia induced by orofacial inflammation combined with stress in adult female rats [J]. Eur J Pharmacol, 2021, 913: 174619.
[22] ARNAL J F, LENFANT F, METIVIER R, et al. Membrane and Nuclear Estrogen Receptor Alpha Actions: From Tissue Specificity to Medical Implications [J]. Physiol Rev, 2017, 97(3): 1045-87.
[23] CHEN Q, ZHANG W, SADANA N, et al. Estrogen receptors in pain modulation: cellular signaling [J]. Biol Sex Differ, 2021, 12(1): 22.
[24] JIAO Y, GAO P, DONG L, et al. Molecular identification of bulbospinal ON neurons by GPER, which drives pain and morphine tolerance [J]. J Clin Invest, 2023, 133(1).
[25] JIE LUO X H, YALI LI, YANG LI, XUEQIN XU, YAN GAO, RUOSHI SHI, WANJUN YAO, JUYING LIU, CHANGBIN KE. GPR30 disrupts the balance of GABAergic and glutamatergic transmission in the spinal cord driving to the development of bone cancer pain [J]. Oncotarget, 2016, 7(45): 73462-72.
[26] TAKANAMI K, SAKAMOTO H, MATSUDA K, et al. Expression of G protein-coupled receptor 30 in the spinal somatosensory system [J]. Brain Res, 2010, 1310: 17-28.
[27] QI L, LIN S H, MA Q. Spinal VGLUT3 lineage neurons drive visceral mechanical allodynia but not sensitized visceromotor reflexes [J]. Neuron, 2023, 111(5): 669-81 e5.
[28] STEPHANIE C KOCH D A A M G. Spinal Circuits for Touch, Pain, and Itch [J]. Annual Review of Physiology, 2018.
[29] CAI B, WU D, XIE H, et al. A direct spino-cortical circuit bypassing the thalamus modulates nociception [J]. Cell Res, 2023, 33(10): 775-89.
[30] WU Z H, SHAO H Y, FU Y Y, et al. Descending Modulation of Spinal Itch Transmission by Primary Somatosensory Cortex [J]. Neurosci Bull, 2021, 37(9): 1345-50.
[31] ZHANG W, WU H, XU Q, et al. Estrogen modulation of pain perception with a novel 17beta-estradiol pretreatment regime in ovariectomized rats [J]. Biol Sex Differ, 2020, 11(1): 2.
[32] DENG C, GU Y J, ZHANG H, et al. Estrogen affects neuropathic pain through upregulating N-methyl-D-aspartate acid receptor 1 expression in the dorsal root ganglion of rats [J]. Neural Regen Res, 2017, 12(3): 464-9.
[33] WANG J, WANG S, FANG Z, et al. Estrogen receptor GPR30 in the anterior cingulate cortex mediates exacerbated neuropathic pain in ovariectomized mice [J]. Brain Res, 2024: 148798.
[34] LI J, GAO P, ZHANG S, et al. The G protein-coupled estrogen receptor of the trigeminal ganglion regulates acute and chronic itch in mice [J]. CNS Neurosci Ther, 2024, 30(2): e14367.
[35] JIANG M, SUN Y, LEI Y, et al. GPR30 receptor promotes preoperative anxiety-induced postoperative hyperalgesia by up-regulating GABA(A)-alpha4beta1delta subunits in periaqueductal gray in female rats [J]. BMC Anesthesiol, 2020, 20(1): 93.
[36] LIU S B, TIAN Z, GUO Y Y, et al. Activation of GPR30 attenuates chronic pain-related anxiety in ovariectomized mice [J]. Psychoneuroendocrinology, 2015, 53: 94-107.
[37] TIAN Z, WANG Y, ZHANG N, et al. Estrogen receptor GPR30 exerts anxiolytic effects by maintaining the balance between GABAergic and glutamatergic transmission in the basolateral amygdala of ovariectomized mice after stress [J]. Psychoneuroendocrinology, 2013, 38(10): 2218-33.
[38] AN G, LI W, YAN T, et al. Estrogen rapidly enhances incisional pain of ovariectomized rats

primarily through the G protein-coupled estrogen receptor [J]. Int J Mol Sci, 2014, 15(6): 10479-91.

[39] DELIU E, BRAILOIU G C, ARTERBURN J B, et al. Mechanisms of G protein-coupled estrogen receptor-mediated spinal nociception [J]. J Pain, 2012, 13(8): 742-54.

[40] XIANG H C, LIN L X, HU X F, et al. AMPK activation attenuates inflammatory pain through inhibiting NF-kappaB activation and IL-1beta expression [J]. J Neuroinflammation, 2019, 16(1): 34.

[41] VACCA V, MARINELLI S, PIERONI L, et al. Higher pain perception and lack of recovery from neuropathic pain in females: a behavioural, immunohistochemical, and proteomic investigation on sex-related differences in mice [J]. Pain, 2014, 155(2): 388-402.

[42] VACCA V, MARINELLI S, PIERONI L, et al. 17beta-estradiol counteracts neuropathic pain: a behavioural, immunohistochemical, and proteomic investigation on sex-related differences in mice [J]. Sci Rep, 2016, 6: 18980.

[43] ZHANG Y, LU N, ZHAO Z Q, et al. Involvement of estrogen in rapid pain modulation in the rat spinal cord [J]. Neurochem Res, 2012, 37(12): 2697-705.

[44] SWETHA E MURTHY M C L, IHAB DAOU, KARA L MARSHALL, FREDERICK SCHWALLER, JOHANNES KüHNEMUND, ALLAIN G FRANCISCO, WILLIAM T KEENAN, ADRIENNE E DUBIN, GARY R LEWIN, ARDEM PATAPOUTIAN. The mechanosensitive ion channel Piezo2 mediates sensitivity to mechanical pain in mice [J]. Science Translational Medicine, 2018, 10: eaat9897.

[45] ALICE ARCOURT S G L. Peripheral and spinal circuits involved in mechanical allodynia [J]. Pain, 2015, 156(2): 220-1.

[46] ZHANG Y, XIAO X, ZHANG X M, et al. Estrogen facilitates spinal cord synaptic transmission via membrane-bound estrogen receptors: implications for pain hypersensitivity [J]. J Biol Chem, 2012, 287(40): 33268-81.

[47] CAO B, SCHERRER G, CHEN L. Spinal cord retinoic acid receptor signaling gates mechanical hypersensitivity in neuropathic pain [J]. Neuron, 2022, 110(24): 4108-24 e6.

[48] DAVID S BREDT R A N. AMPA receptor trafficking at excitatory synapses [J]. Neuron, 2003, 40(2): 361-79.

[49] BASBAUM A I, BAUTISTA D M, SCHERRER G, et al. Cellular and molecular mechanisms of pain [J]. Cell, 2009, 139(2): 267-84.

[50] FRANK PORRECA M H O A G F G. Chronic pain and medullary descending facilitation [J]. TRENDS in Neurosciences, 2002, 25(6).

[51] SHANNON E. BURGESS L R G, MICHAEL H. OSSIPOV, T. PHILIP MALAN JR, TODD W. VANDERAH,, JOSEPHINE LAI A F P. Time-Dependent Descending Facilitation from the Rostral Ventromedial Medulla Maintains, But Does Not Initiate, Neuropathic Pain [J]. The Journal of Neuroscience, 2002, 22(12): 5129–36.

[52] L. R. GARDELL T W V, S. E. GARDELL, R. WANG, M. H. OSSIPOV, J. LAI, AND F. PORRECA. Enhanced Evoked Excitatory Transmitter Release in Experimental Neuropathy Requires Descending Facilitation [J]. The Journal of Neuroscience, 2003, 23(23): 8370 – 9.

[53] BEE L A, DICKENSON A H. Rostral ventromedial medulla control of spinal sensory processing in normal and pathophysiological states [J]. Neuroscience, 2007, 147(3): 786-93.

[54] BANNISTER K, DICKENSON A H. The plasticity of descending controls in pain: translational probing [J]. J Physiol, 2017, 595(13): 4159-66.

[55] LAU B K, VAUGHAN C W. Descending modulation of pain: the GABA disinhibition hypothesis of analgesia [J]. Curr Opin Neurobiol, 2014, 29: 159-64.

[56] DIXON W J. EFFICIENT ANALYSIS OF EXPERIMENTAL OBSERVATIONS [J]. Ann Rev Pharmacol Toxicol, 1980.

[57] WINTERS B L, RAWLING T, VANDENBERG R J, et al. Activity of novel lipid glycine transporter inhibitors on synaptic signalling in the dorsal horn of the spinal cord [J]. Br J Pharmacol, 2018, 175(12): 2337-47.

704 **Figure Legends**

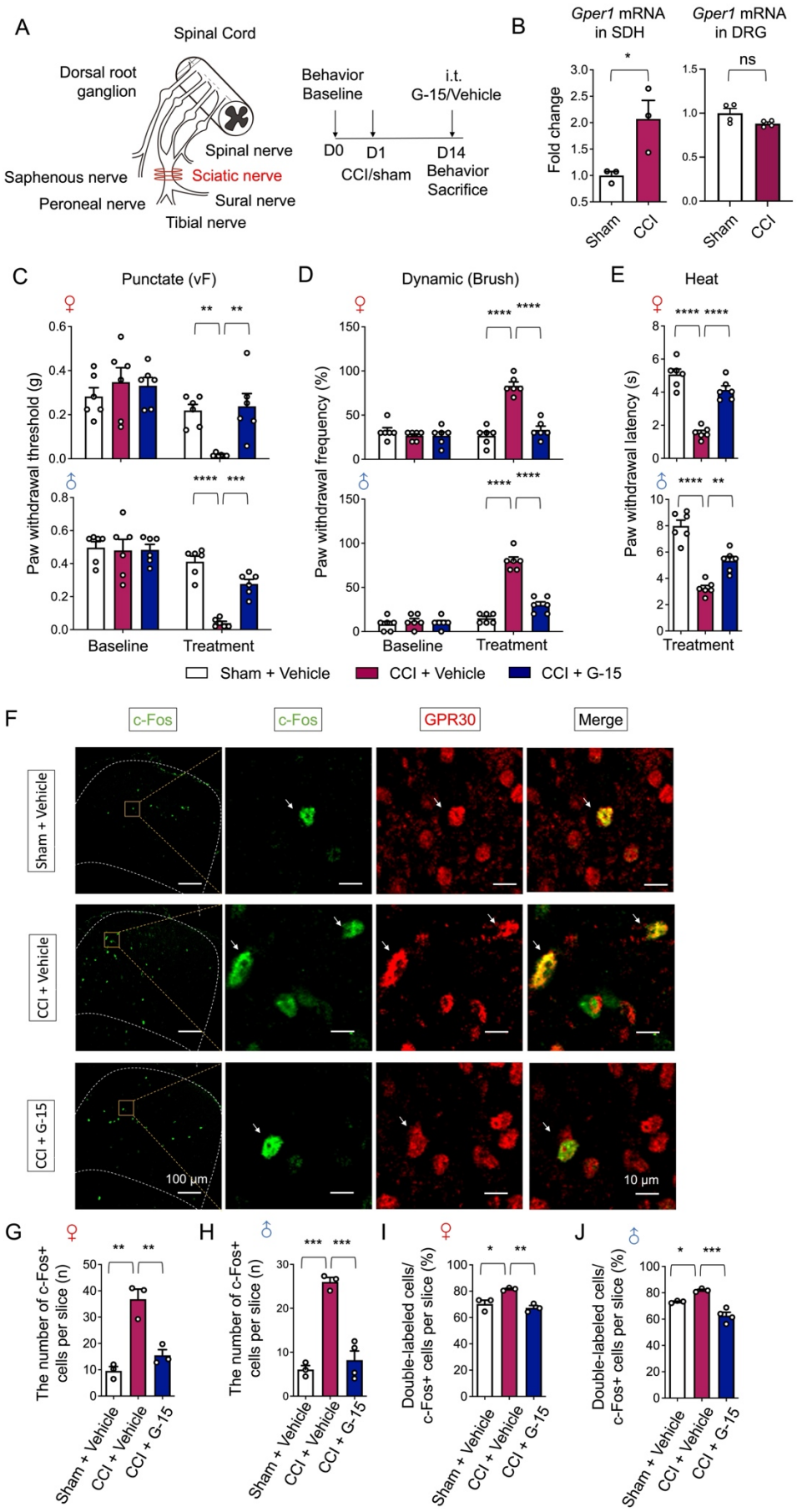
A
Spinal Cord
Dorsal root ganglion
Spinal nerve
Saphenous nerve
Sciatic nerve
Peroneal nerve
Sural nerve
Tibial nerve
Behavior Baseline
i.t. G-15/Vehicle
D0
D1
D14
CCI/sham
Behavior Sacrifice
B
Gper1 mRNA in SDH
Gper1 mRNA in DRG
Fold change
ns
Sham
CCI
C
Punctate (vF)
D
Dynamic (Brush)
E
Heat
Paw withdrawal threshold (g)
Paw withdrawal frequency (%)
Paw withdrawal latency (s)
Baseline
Treatment
Sham + Vehicle
CCI + Vehicle
CCI + G-15
F
c-Fos
c-Fos
GPR30
Merge
Sham + Vehicle
CCI + Vehicle
CCI + G-15
100 µm
10 µm
G
The number of c-Fos+ cells per slice (n)
H
The number of c-Fos+ cells per slice (n)
I
Double-labeled cells/ c-Fos+ cells per slice (%)
J
Double-labeled cells/ c-Fos+ cells per slice (%)
Sham + Vehicle
CCI + Vehicle
CCI + G-15

705

Figure 1. CCI-induced neuropathic pain and neuronal activation were reversed by spinal inhibition of GPR30.

A Schematic illustration of CCI surgery for induction of neuropathic pain (Left) and diagram showing the timeline of CCI surgery, drug administration and behavioral tests (Right).

B Quantitative PCR analysis of *Gper1* mRNA in SDH from sham and CCI mice (Left, n = 3 mice for each group) and *Gper1* mRNA in DRG from sham and CCI mice (Right, n = 4 mice for each group).

C-E Behavioral tests of basic nociception and 14 days after CCI or sham surgery along with intrathecal injection of antagonist of GPR30 or vehicle in Von Frey tests **(C)**, Brush tests **(D)** and Heat tests **(E)** in mice of both sexes (n = 6 mice for each group).

F Immunochemical detection of c-Fos (Green) and GPR30 (Red). Scale bars: 100 μm. Boxed area of images is enlarged on the right. Scale bars: 10 μm. White arrows indicate double-positive cells.

G, H Total number of c-Fos positive neurons in the SDH per section in female mice **(G)** and male mice **(H)** (n = 3-4 mice for each group, 4-6 pictures were analyzed for each mouse).

I, J Percentage of c-Fos positive neurons expressing GPR30 in female mice **(I)** and male mice **(J)**. (n = 3-4 mice for each group, 4-6 pictures were analyzed for each mouse).

Data information: in **(B)**, *P < 0.05 (Unpaired Student's t-test). In **(C, D)**, **P < 0.01; ***P < 0.001; ****P < 0.0001 (two-way ANOVA with Turkey's multiple comparisons test). In **(E)**, **P < 0.01; ****P < 0.0001 (one-way ANOVA with Turkey's multiple comparisons test). In **(G-J)**, *P < 0.05; **P < 0.01; ***P < 0.001 (one-way ANOVA with Turkey's multiple comparisons test). All data are presented as mean ± SEM.

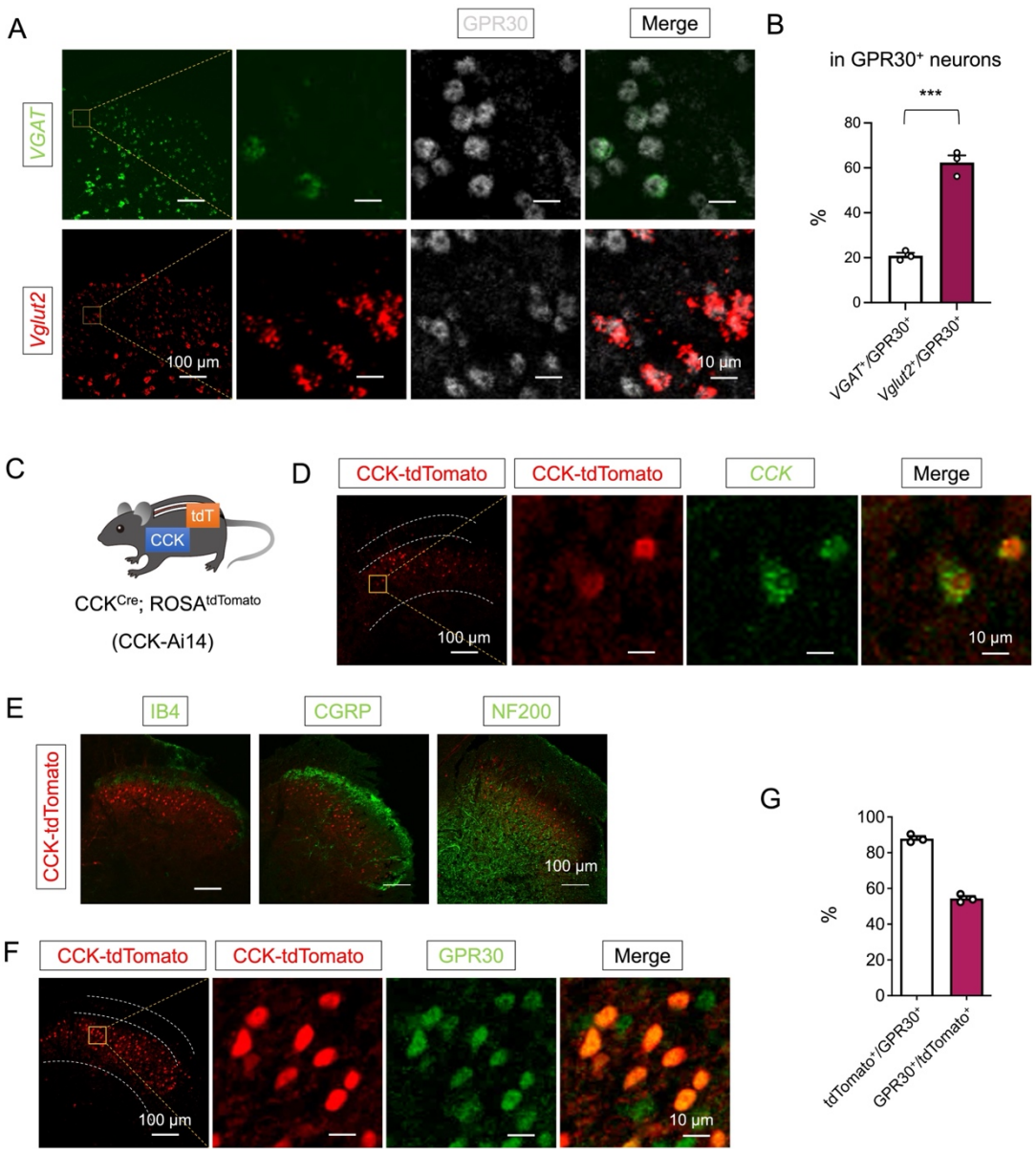

Figure 2. GPR30 was widely expressed in the CCK^{+} excitatory interneurons in the SDH.

A In situ hybridization showing *VGAT* (Green) and *Vglut2* (Red) with GPR30 (Gray) in the SDH. Scale bar: 100 μm. Boxed area of image is enlarged on the right. Scale bars: 10 μm.

B Percentage of GPR30 positive neurons expressing *VGAT* or *Vglut2* in wild mice. (n = 3 mice, 3-4 pictures were analyzed for each mouse)

C CCK^{Cre} mice express tdTomato in a Cre-dependent manner.

D In situ hybridization showing CCK (Green) with tdTomato (Red) in the SDH. Scale bar: 100 μm. Boxed area of image is enlarged on the right. Scale bars: 10 μm.

737 **E** Double staining of tdTomato^{+} neurons (Red) with IB4, CGRP or NF200 (Green) by

738 immunochemistry. Scale bars: 100 μm.

739 **F** Immunofluorescence in SDH to verify the co-localization of tdTomato^{+} neurons (Red) with

740 GPR30 (Green). Scale bars: 100 μm. Boxed area of images is enlarged on the right. Scale bars:

741 10 μm.

742 **G** Percentage of double labeled neurons in CCK-tdTomato and GPR30 positive neurons. (n =

743 3 mice, 3 pictures were analyzed for each mouse)

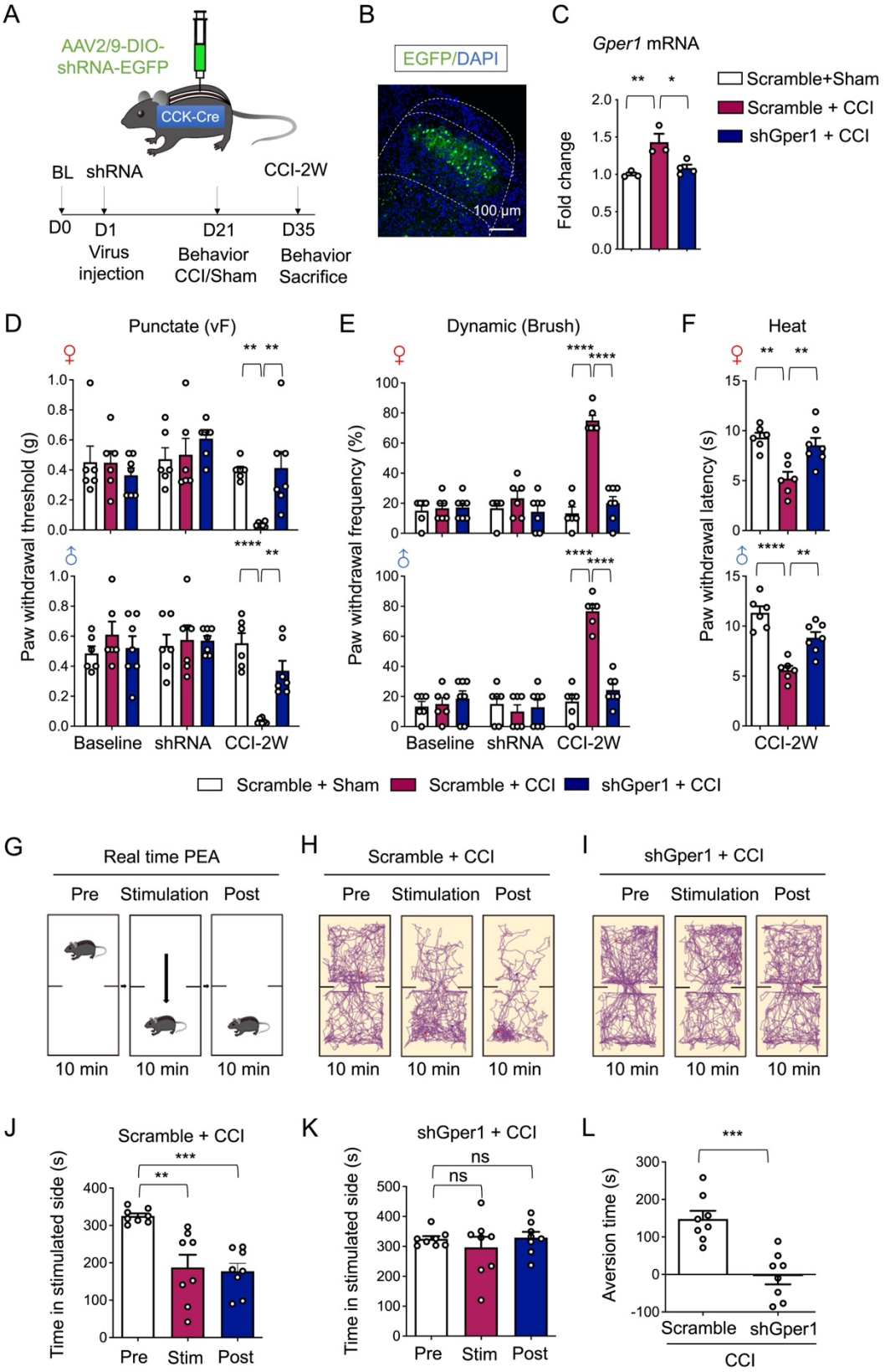
A
AAV2/9-DIO-shRNA-EGFP
CCK-Cre
BL
shRNA
CCI-2W
D0
D1
D21
D35
Virus injection
Behavior CCI/Sham
Behavior Sacrifice
B
EGFP/DAPI
100 μm
C
Gper1 mRNA
Fold change
Scramble+Sham
Scramble + CCI
shGper1 + CCI
D
Punctate (vF)
Paw withdrawal threshold (g)
Baseline
shRNA
CCI-2W
E
Dynamic (Brush)
Paw withdrawal frequency (%)
F
Heat
Paw withdrawal latency (s)
Scramble + Sham
Scramble + CCI
shGper1 + CCI
G
Real time PEA
Pre
Stimulation
Post
10 min
H
Scramble + CCI
I
shGper1 + CCI
J
Scramble + CCI
Time in stimulated side (s)
Pre
Stim
Post
K
shGper1 + CCI
ns
L
Aversion time (s)
Scramble
shGper1
CCI

745 **Figure 3. Knockdown of GPR30 in spinal CCK^+ neurons alleviated neuropathic pain in**

746 **CCI mice.**

747 **A** Schematic illustration of the strategy to knock down Gper1 in the spinal CCK^+ neurons in a

748 Cre-dependent manner (Up) and the diagram showing the timeline of virus injection, CCI

749 surgery and behavioral tests (Down).

750 **B** Immunochemical detection of the localization of virus expression (Green). Scale bars: 100

751 μm.

752 **C** Quantitative PCR analysis of Gper1 mRNA in SDH from sham and CCI mice with

753 intraspinal virus injection (n = 3-4 mice for each group).

754 **D-F** Behavioral tests of basic nociception, 21 days after spinal virus injection and 14 days

755 after CCI or sham surgery along with intrathecal injection of antagonist of GPR30 or vehicle

756 in Von Frey tests **(D)**, Brush tests **(E)** and Heat tests **(F)** in mice of both sexess (n = 6-7 mice

757 for each group).

758 **G** Schematic illustration of real-time place escape/avoidance (PEA) test.

759 **H, I** Representative spatial tracking maps showing the location of a Scramble + CCI group

760 mice **(H)** and a shGper1 + CCI group mice **(I)** before, during and after mechanical stimulation

761 of hind paw in the chambers.

762 **J** Quantification of time the Scramble + CCI group mice spent in preferred chamber before,

763 during and after stimulation (n = 8 mice).

764 **K** Quantification of time the shGper1 + CCI group mice spent in preferred chamber before,

765 during and after stimulation (n = 8 mice).

L Quantification of the aversion time of mice. (time spent in preferred chamber after stimulation minus the time spent before stimulation) (n = 8 mice for each group).

Data information: in **(C)**, *P < 0.05; **P < 0.01 (one-way ANOVA with Turkey's multiple comparisons test). In **(D, E)**, **P < 0.01; ****P < 0.0001 (two-way ANOVA with Turkey's multiple comparisons test). In **(F)**, **P < 0.01; ****P < 0.0001 (one-way ANOVA with Turkey's multiple comparisons test). In **(J, K)**, *P < 0.05; **P < 0.01; ***P < 0.001; ns = not significant. (one-way ANOVA with Turkey's multiple comparisons test). In **(L)**, ***P < 0.001 (Unpaired Student's t-test). All data are presented as mean ± SEM.

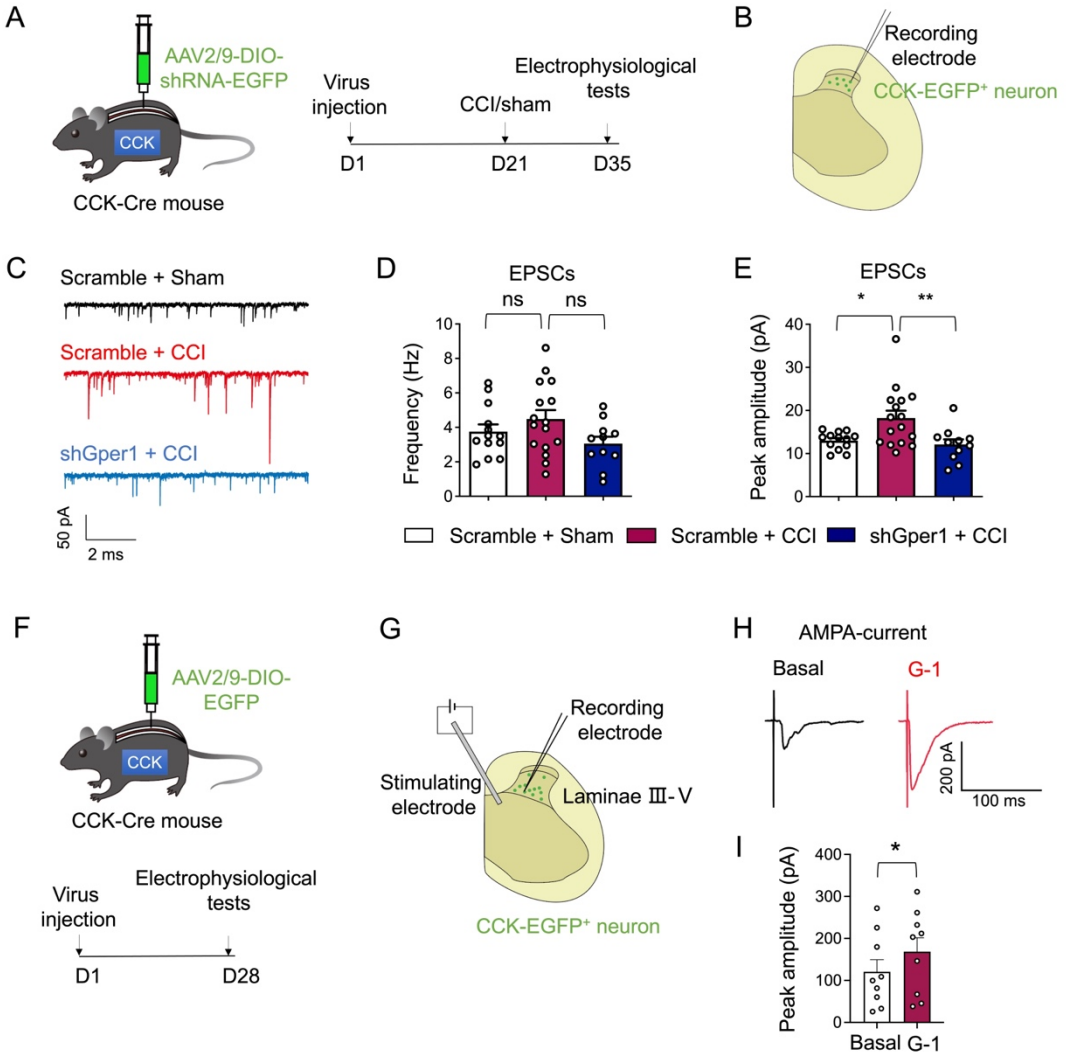

Figure 4. Knockdown of GPR30 in spinal CCK$^+$ neurons reverse the enhancement of sEPSC in CCI mice

A Schematic illustration of the strategy to knock down Gper1 in the spinal CCK$^+$ neurons in a Cre-dependent manner (Left) and the diagram showing the timeline of virus injection, CCI surgery and electrophysiological tests (Right).

B Schematic illustration of spinal slice electrophysiological recordings from CCK-EGFP neurons located in the deep laminae of SDH.

782 **C** Representative spontaneous EPSCs in CCK-EGFP neurons.

783 **D** The frequency of spontaneous EPSCs.

784 **E** The peak amplitude spontaneous EPSCs (n = 10-16 cells from 5 mice per group).

785 **F** Schematic illustration of the strategy to visualize CCK^+ neurons in a Cre-dependent manner

786 (Up) and the diagram showing the timeline of virus injection and electrophysiological tests

787 (Down).

788 **G** Schematic illustration of spinal slice electrophysiological recordings from $CCK\text{-}EGFP^+$

789 neurons located in the deep laminae of SDH during electric stimulation of the deep laminae of

790 SDH to simulate APMA currents.

791 **H** Representative AMPA-current in $CCK\text{-}EGFP^+$ neurons before and after administration of

792 G-1 (0.1 μM).

793 **I** The peak amplitude AMPA currents before and after administration of G-1 (n = 8 cells from

794 4 mice).

795 Data information: in **(D, E)**, *P < 0.05; **P < 0.01; ns = not significant (one-way ANOVA with

796 Turkey's multiple comparisons test). In **(I)**, *P < 0.05 (Paired Student's t-test). All data are

797 presented as mean ± SEM.

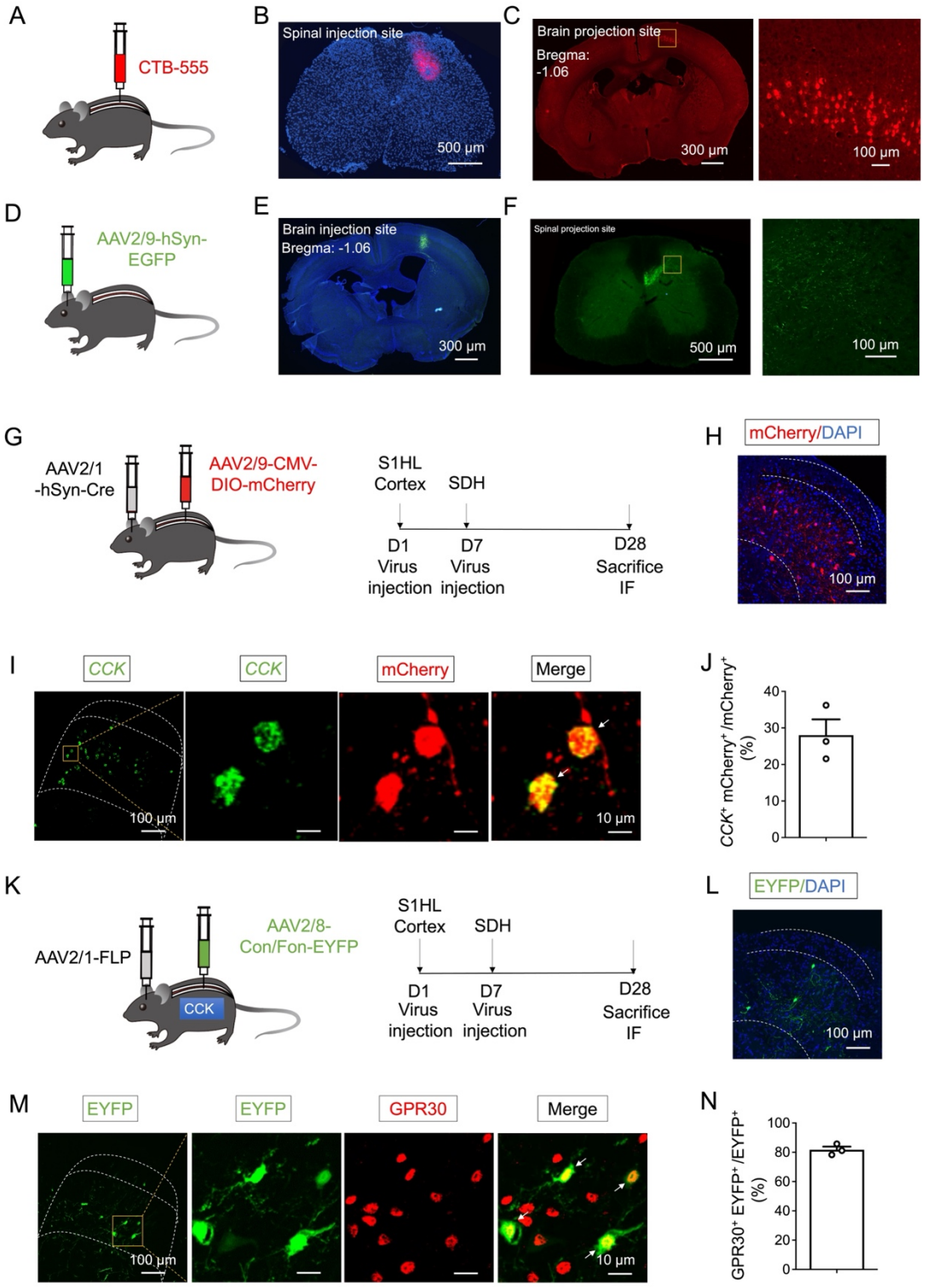

Figure 5. GPR30 was expressed in the spinal CCK$^+$ neurons receiving direct projection from S1 cortex.

A Schematic illustration of the strategy to retrograde tracing the projections innervating spinal dorsal horn via CTB-555.

B Fluorescence image showing the site of CTB-555 injection in the spinal dorsal horn. Scale bars: 500 μm.

C Coronal brain section showing the location of tdTomato+ neurons in the S1HL cortex. Scale bars: 300 μm. Boxed area of image is enlarged on the right. Scale bars: 100 μm.

D Schematic illustration of the strategy to anterograde tracing the projections from S1HL cortex.

E Coronal brain section showing the site of AAV injection in the S1HL cortex. Scale bars: 300 μm.

F Fluorescence image showing the S1HL-SDH tract terminates in the deep laminae of spinal dorsal horn. Scale bars: 500 μm. Boxed area of image is enlarged on the right. Scale bars: 100 μm.

G Schematic illustration of the strategy for identifying the spinal post-synaptic neurons of S1-SDH projections (Left) and diagram showing the timeline of AAV2/1 injection in the S1HL cortex, AAV2/9 injection in the spinal dorsal horn and immunofluorescence (Right).

H Representative image showing the mCherry^{+} post-synaptic neurons of the S1HL-SDH projections in the deep laminae of SDH. Scale bars: 100 μm.

I In situ hybridization showing CCK (Green) with RFP (Red) by immunofluorescence in the spinal dorsal horn. Scale bars: 100 μm. Boxed area of image is enlarged on the right. Scale bars: 10 μm. White arrows indicate double-positive cells.

822 **J** About 28.13% of RFP^+ post-synaptic neurons of S1HL-SDH projections expressing CCK (n

823 = 3 mice, 3 pictures were analyzed for each mouse).

824 **K** Schematic illustration of the strategy for identifying the spinal CCK^+ post-synaptic neurons

825 of S1HL-SDH projections in CCK^{Cre} mice (Left) and diagram showing the timeline of

826 AAV2/1 injection in the S1HL cortex, AAV2/9 injection in the spinal dorsal horn and

827 immunofluorescence (Right).

828 **L** Representative image showing the $EGFP^+$ CCK^+ post-synaptic neurons of the S1-SDH

829 projections in the spinal dorsal horn with DAPI. Scale bars: 100 μm.

830 **M** Double staining of $EGFP^+$ neurons with GPR30 by immunohistochemistry. Scale bars: 100

831 μm. Boxed area of image is enlarged on the right. Scale bars: 10 μm.

832 **N** About 81.7% of CCK+ post-synaptic neurons of S1HL-SDH projections expressing GPR30

833 (n = 3 mice, 7-18 pictures were analyzed for each mouse).

834 Data information: in **(J, N)**, data are presented as mean ± SEM.

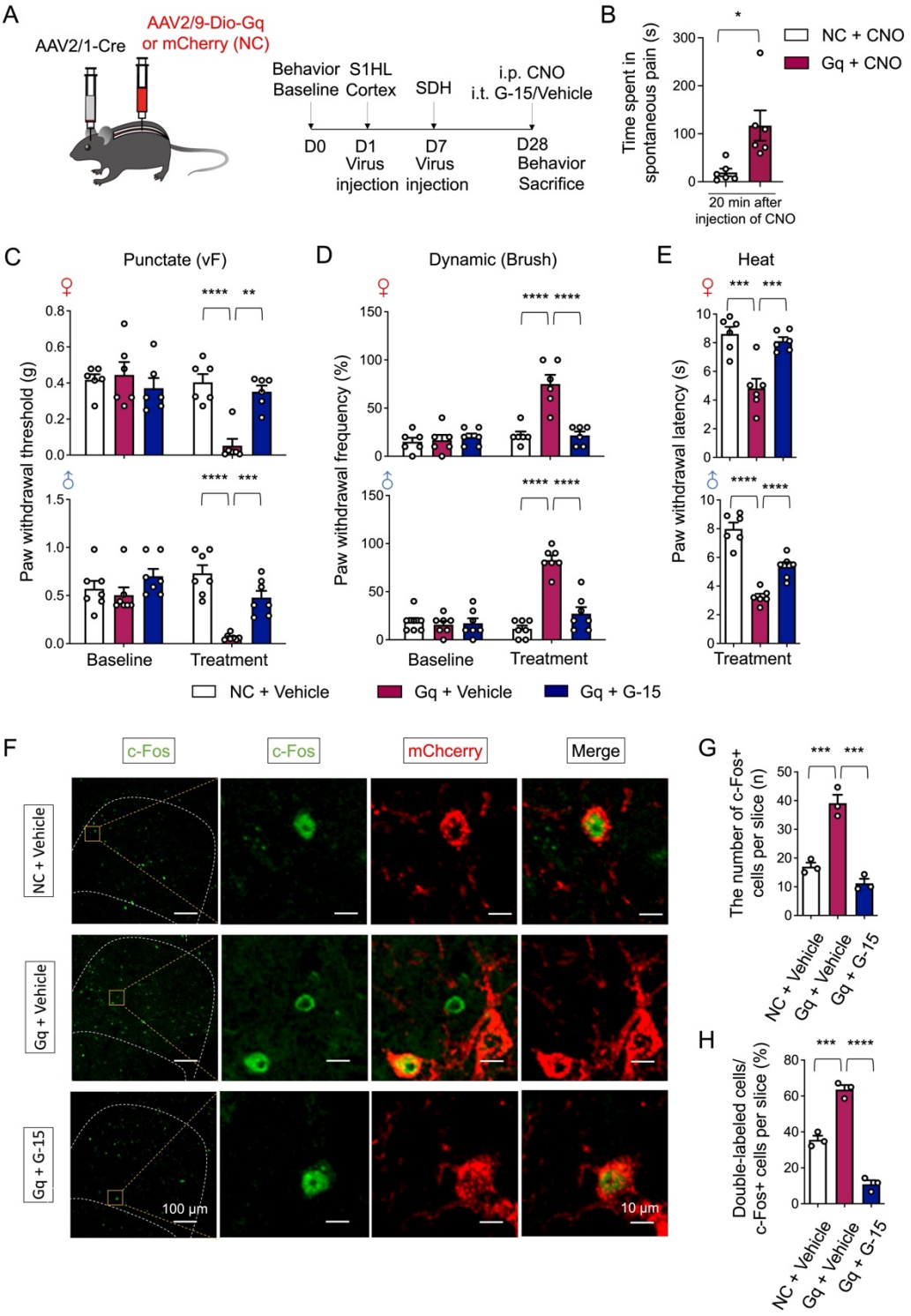

Figure 6. Chemogenetic activation of S1-SDH post-synaptic neurons mimicked neuropathic pain symptoms, which were reversed by spinal inhibition of GPR30.

A Schematic illustration of the strategy for identifying the post-synaptic neurons of S1HL-SDH

projections in SDH (Left) and diagram showing the timeline of AAV2/1 injection in the S1HL cortex, AAV2/9 injection in the spinal dorsal horn and behavioral tests (Right).

B Spontaneous pain induced by intraperitoneal injection of CNO within 20 min (n = 6 mice for each group).

C-E Behavioral tests of basic nociception, 28 days after brain virus injection along with intraperitoneal injection of CNO and intrathecal injection of antagonist of GPR30 or vehicle in Von Frey tests **(C)**, Brush tests **(D)** and Heat tests **(E)** in mice of both sexess (n = 6 mice for each group).

F Immunochemical detection of c-Fos (Green) and m-Cherry+ post-synaptic neurons (Red). Scale bars: 100 μm. Boxed area of images is enlarged on the right. Scale bars: 10 μm.

G Total number of c-Fos positive neurons in the SDH per section (n = 3 mice for each group, 3 pictures were analyzed for each mouse). **H** Percentage of c-Fos positive neurons expressed in m-Cherry (n = 3 mice for each group, 3 pictures were analyzed for each mouse).

Data information: in **(B)**, *P < 0.05 (Unpaired Student's t-test). In **(C, D)**, **P < 0.01; ***P < 0.001; ****P < 0.0001 (two-way ANOVA with Turkey's multiple comparisons test). In **(E)**, ***P < 0.001; ****P < 0.0001 (one-way ANOVA with Turkey's multiple comparisons test). In **(G, H)**, ***P < 0.001; ****P < 0.0001. (one-way ANOVA with Turkey's multiple comparisons test). All data are presented as mean ± SEM.

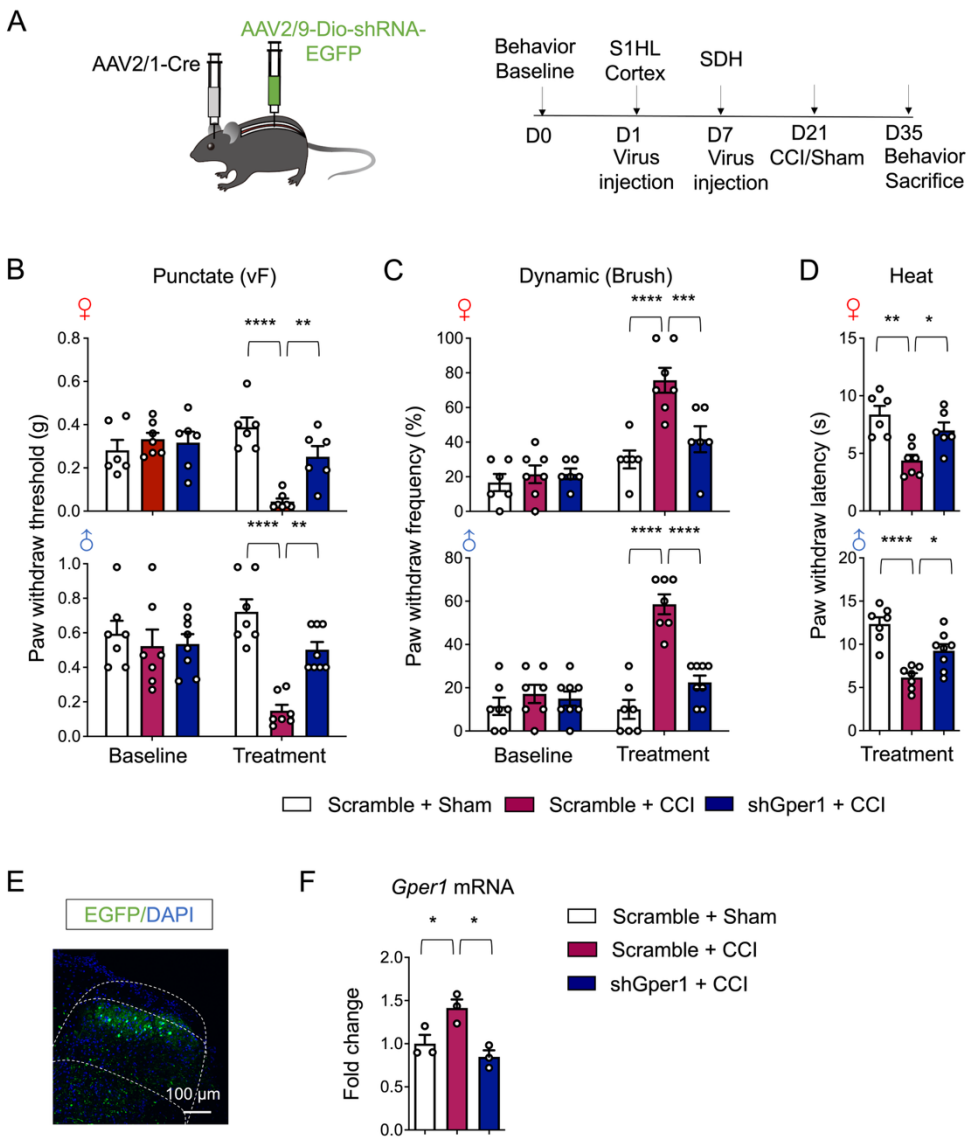

Figure 7. CCI-induced neuropathic pain was attenuated by knock-down of GPR30 in S1-SDH post-synaptic neurons.

A Schematic illustration of the strategy to knock down Gper1 in the post-synaptic neurons of S1HL-SDH projections in a Cre-dependent manner (Up) and the diagram showing the timeline of virus injection, CCI surgery and behavioral tests (Down).

B-D Behavioral tests of basic nociception and 14 days after CCI surgery in Von Frey tests **(B)**, Brush tests **(C)** and Heat tests **(D)** in mice of both sexess (n = 6 mice for each group).

865 **E** Immunochemical detection of the localization of virus expression (Green). Scale bars: 100

866 μm.

867 **F** Quantitative PCR analysis of Gper1 mRNA in SDH (n = 3 mice for each group).

868 Data information: in **(B, C)**, **P < 0.01; ***P < 0.001; ****P < 0.0001 (two-way ANOVA

869 with Turkey's multiple comparisons test). In **(D)**, *P < 0.05; **P < 0.01; ****P < 0.0001 (one-

870 way ANOVA with Turkey's multiple comparisons test). In **(F)**, *P < 0.05 (one-way ANOVA

871 with Turkey's multiple comparisons test). All data are presented as mean ± SEM.

872

Supplemental Figure Legends

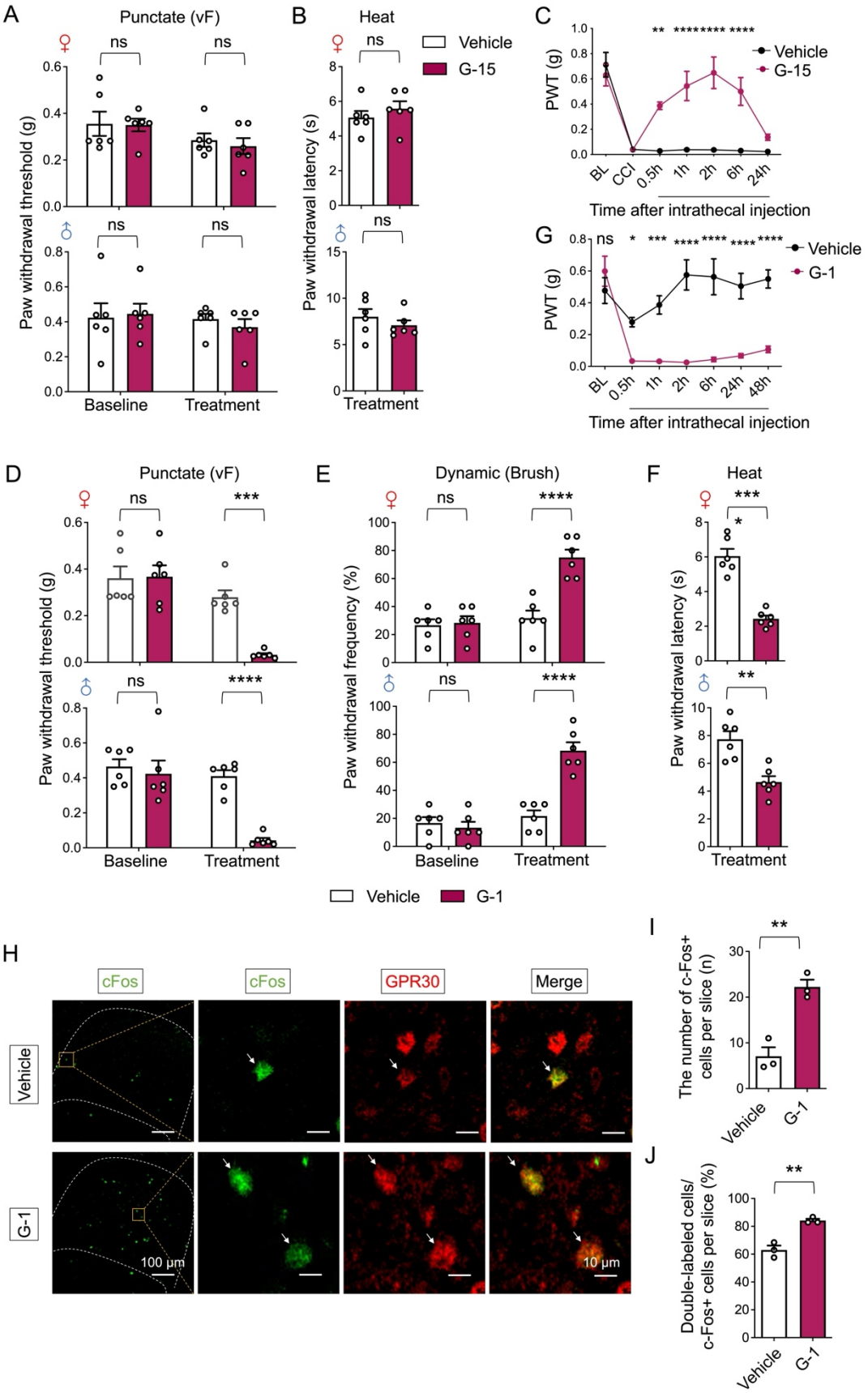

Figure S1. Spinal inhibition of GPR30 did not change the basic nociception while spinal activation of GPR30 mimicked neuropathic pain symptoms in naïve mice

A, B Behavioral tests of nociception before and after intrathecal injection of G-15 or vehicle in Von Frey tests **(A)** and Heat tests **(B)** in naive mice of both sexess (n = 6 mice for each group).

C Time course of Von Frey tests after intrathecal injection of G-15 or vehicle in CCI mice (n = 6 mice for each group).

D-F Behavioral tests of nociception before and after intrathecal injection of G-1 or vehicle in Von Frey tests **(D)**, Brush tests **(E)** and Heat tests **(F)** in naive mice of both sexess (n = 6 mice for each group).

G Time course of Von Frey tests after intrathecal injection of G-1 or vehicle in naive mice (n = 6 mice for each group).

H Immunochemical detection of c-Fos (Green) and GPR30 (Red). Scale bars: 100 μm. Boxed area of images is enlarged on the right. Scale bars: 10 μm. White arrows indicate double-positive cells.

I Total number of c-Fos positive neurons in the SDH per section (n = 3 mice for each group, 3-5 pictures were analyzed for each mouse).

J Percentage of c-Fos positive neurons expressing GPR30 (n = 3 mice for each group, 3-5 pictures were analyzed for each mouse).

Data information: in **(A)**, ns = not significant (two-way ANOVA with Turkey's multiple comparisons test). In **(B)**, ns = not significant (Unpaired Student's t-test). In **(C)**, **P < 0.01; ****P < 0.0001; ns = not significant (two-way ANOVA with Turkey's multiple comparisons test). In **(D, E)**, ***P < 0.001; ****P < 0.0001; ns = not significant. (two-way ANOVA with

Turkey's multiple comparisons test). In **(F)**, **P < 0.01; ****P < 0.0001 (Unpaired Student's t-test). In **(G)**, *P < 0.05; ***P < 0.001; ****P < 0.0001; ns = not significant (two-way ANOVA with Turkey's multiple comparisons test). In **(I, J)**, **P < 0.01 (Unpaired Student's t-test).All data are presented as mean ± SEM.

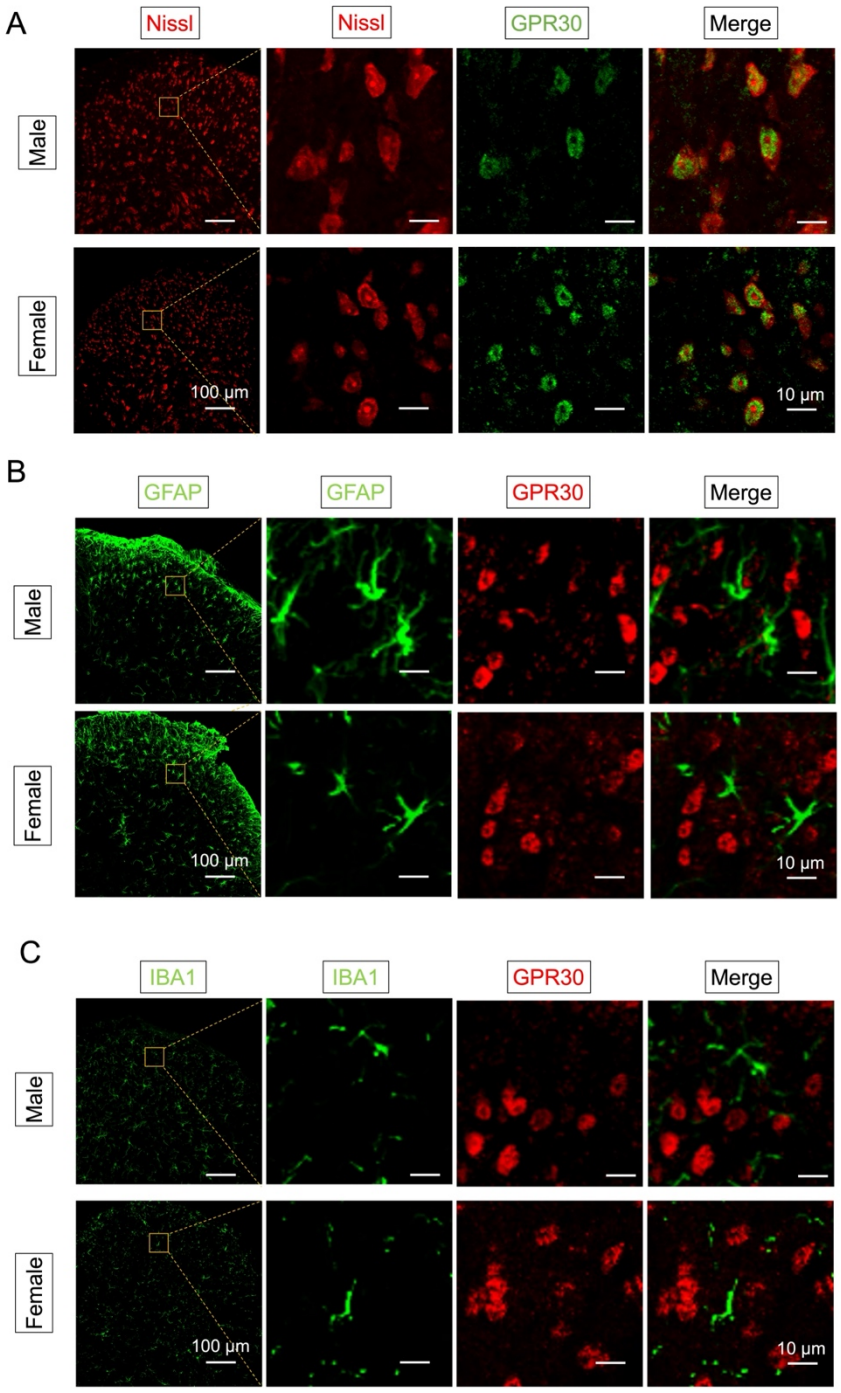
A
Nissl
Nissl
GPR30
Merge
Male
Female
100 µm
10 µm
B
GFAP
GFAP
GPR30
Merge
Male
Female
100 µm
10 µm
C
IBA1
IBA1
GPR30
Merge
Male
Female
100 µm
10 µm

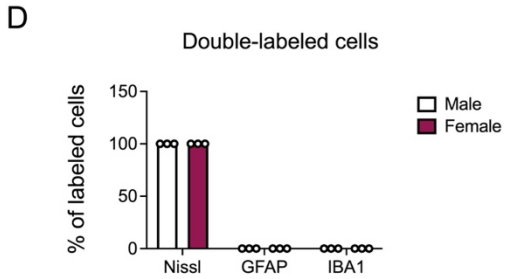
D
Double-labeled cells
% of labeled cells
150
100
50
0
Nissl
GFAP
IBA1
Male
Female

901

902 **Figure S2. GPR30 was mainly expressed in the spinal neurons.**

903 **A** Double-staining of GPR30 (Green) with Nissl (Red) in male (up) and female mice (down).

904 Scale bars: 100 μm. Boxed area of images is enlarged on the right. Scale bars: 10 μm.

905 **B** Double-staining of GPR30 (Red) with GFAP (Green) in male (up) and female mice (down).

906 Scale bars: 100 μm. Boxed area of images is enlarged on the right. Scale bars 10 μm.

907 **C** Double-staining of GPR30 (Red) with IBA1 (Green) in male (up) and female mice (down).

908 Scale bars: 100 μm. Boxed area of images is enlarged on the right. Scale bars: 10 μm.

909 **D** Percentage of GPR30 expressed in neurons, astrocytes and microglia in both sexess of mice

910 (n = 3 mice for each group, 3 pictures were analyzed for each mouse).

911 Data information: in **(D)**, data are presented as mean ± SEM.

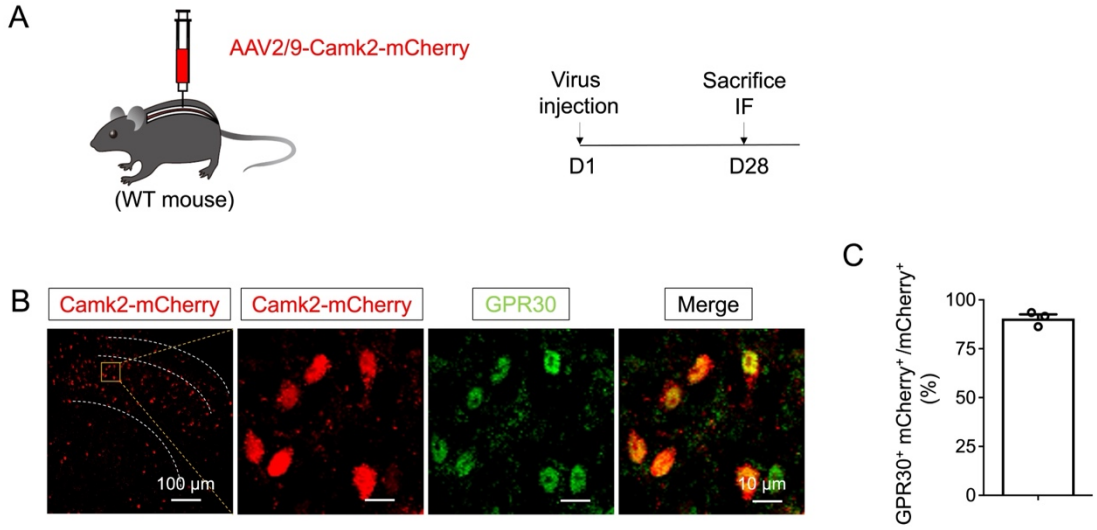

Figure S3. GPR30 was widely expressed in the Camk2$^+$ excitatory interneurons in the SDH.

A Schematic illustration of the strategy to identify the Camk2$^+$ excitatory interneurons in spinal dorsal horn by AAV.

B Double staining of Camk2$^+$ mCherry$^+$ neurons (Red) with GPR30 (Green) by immunohistochemistry. Scale bars: 100 μm. Boxed area of images is enlarged on the right. Scale bars: 10 μm.

C Percentage of Camk2 positive neurons expressing GPR30 in wild mice. (n = 3 mice, 3-4 pictures were analyzed for each mouse)

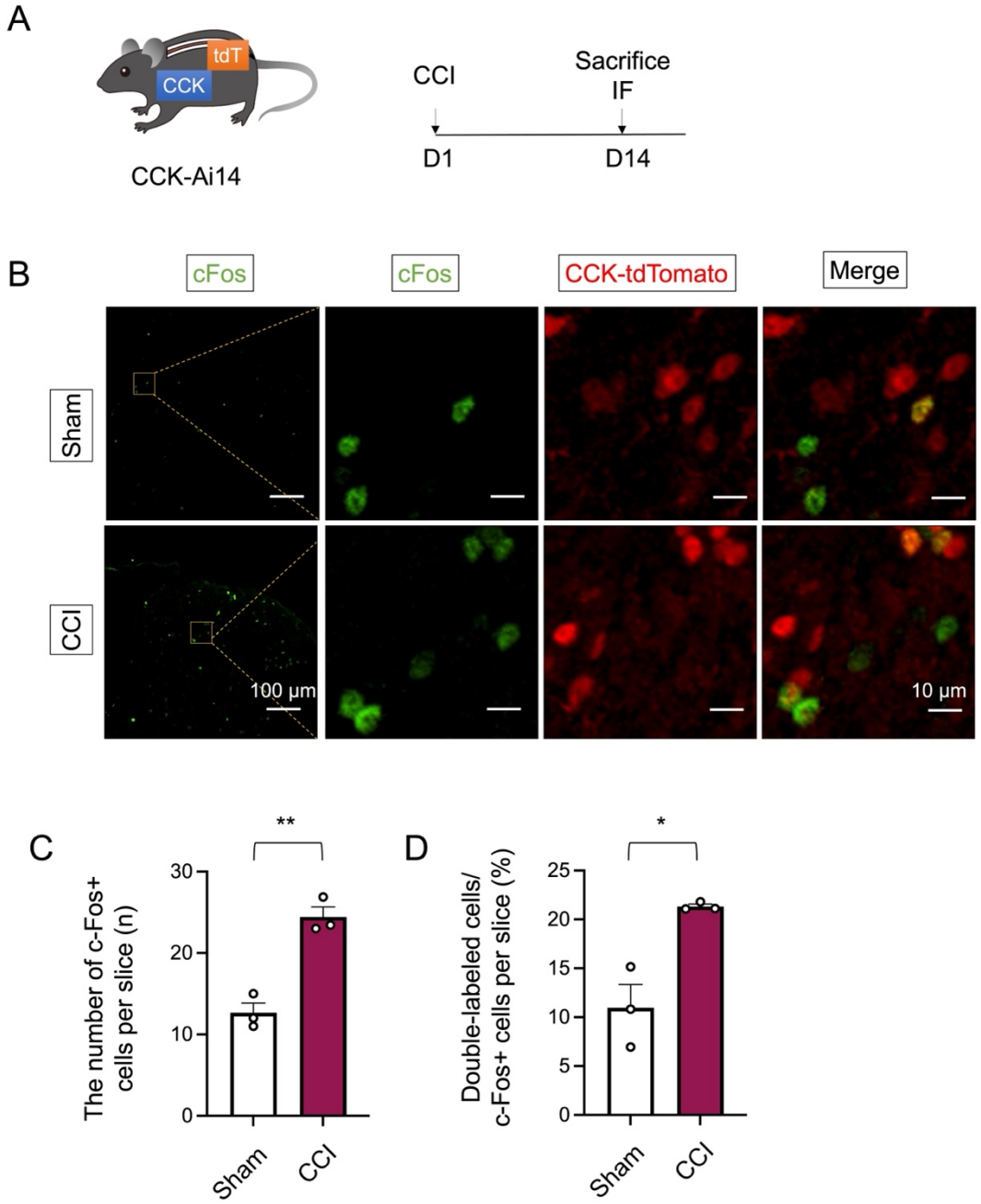

Figure S4. CCK positive neurons were more activated after CCI.

A Schematic illustration of CCK-Ai14 subjected with CCI.

B Immunochemical detection of c-Fos (Green) and CCK-tdTomato (Red). Scale bars: 100 μm. Boxed area of images is enlarged on the right. Scale bars: 10 μm.

C Total number of c-Fos positive neurons in the SDH per section (n = 3 mice for each group, 6-8 pictures were analyzed for each mouse).

930 **D** Percentage of c-Fos positive neurons expressed on CCK-tdTomato positive neurons (n = 3

931 mice for each group, 6-10 pictures were analyzed for each mouse).

932

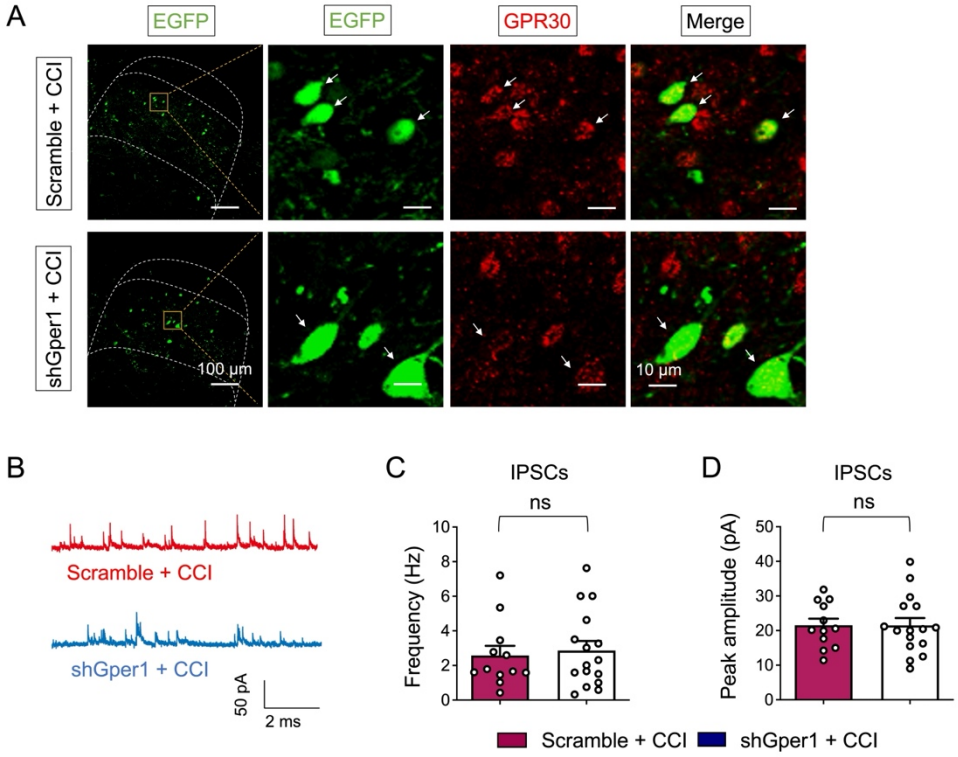

Figure S5. Knockdown of GPR30 in spinal CCK$^+$ neurons did not change the sIPSC in CCI mice.

A Immunohistochemical detection of GPR30 (Red) and shRNA (Green) in mice with virus injection. Note that the intensity of GPR30 fluorescence is less in shGper1-EGFP$^+$ cells than that in scramble-EGFP$^+$ cells. Scale bars: 100 μm. Boxed area of image is enlarged on the right. Scale bars: 10 μm.

B Representative spontaneous IPSCs in CCK-EGFP neurons.

C The frequency of spontaneous IPSCs (n = 12-16 cells from 5 mice).

D The peak amplitude spontaneous IPSCs (n = 12-16 cells from 5 mice).

Data information: in **(C, D)**, ns = not significant (Unpaired Student's t-test). All data are presented as mean ± SEM.

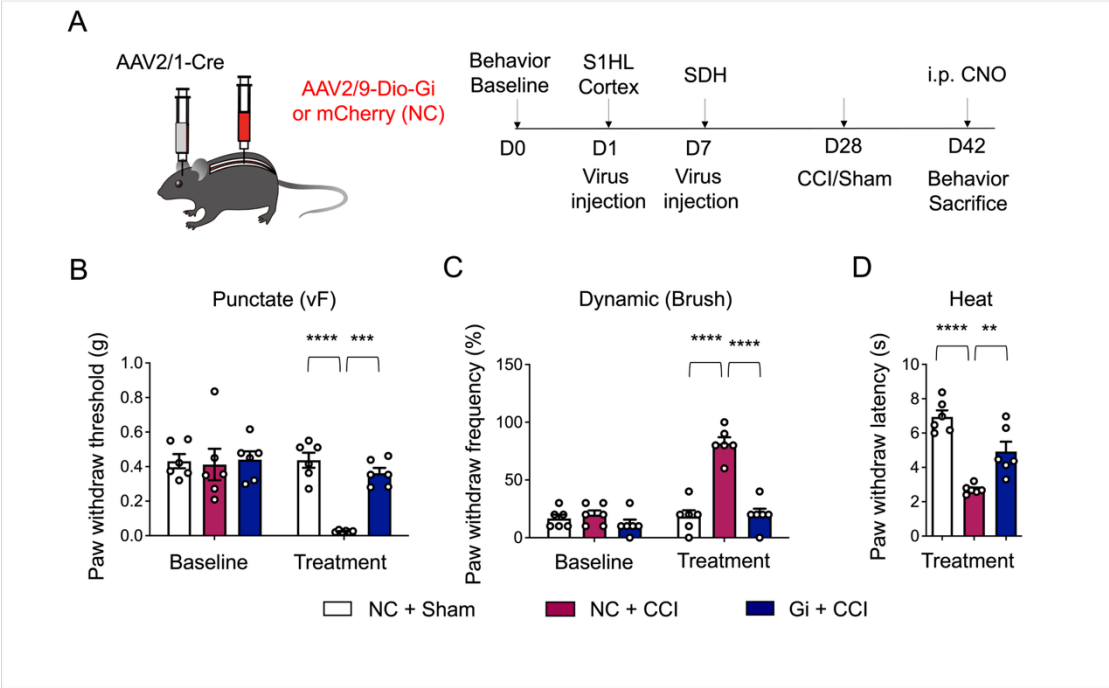

Figure S6. CCI-induced neuropathic pain was relieved by chemogenetic inhibition of S1-SDH post-synaptic neurons.

A Schematic illustration of the strategy for identifying the post-synaptic neurons of S1HL-SDH projections in SDH (Left) and diagram showing the timeline of AAV2/1 injection in the S1HL cortex, AAV2/9 injection in the spinal dorsal horn, CCI surgery and behavioral tests (Right).

B-D Behavioral tests of basic nociception, 14 days after CCI surgery along with intraperitoneal injection of CNO in Von Frey tests **(B)**, Brush tests **(C)** and Heat tests **(D)** in mice (n = 6 mice per group).

Data information: In **(B, C)**, ***P < 0.001; ****P < 0.0001. (two-way ANOVA with Turkey's multiple comparisons test). In **(D)**, **P < 0.01; ****P < 0.0001 (one-way ANOVA with Turkey's multiple comparisons test). All data are presented as mean ± SEM

Supplemental Movie Legends

Movie 1. Heat test of mice subjected with CCI and spinal viral injection.

Movie 2. VonFrey test of mice subjected with CCI and spinal viral injection.

Movie 3. Pre-stimulation phase of RT-PEA test of mice subjected with CCI and shGper1.

Movie 4. Stimulation phase of RT-PEA test of mice subjected with CCI and shGper1.

Movie 5. Post-stimulation phase of RT-PEA test of mice subjected with CCI and shGper1.

Movie 6. Pre-stimulation phase of RT-PEA test of mice subjected with CCI and Scramble.

Movie 7. Stimulation phase of RT-PEA test of mice subjected with CCI and Scramble.

Movie 8. Post-stimulation phase of RT-PEA test of mice subjected with CCI and Scramble.